Experimental Investigations of Radiative Association Processes as Related to Interstellar Chemistry

Dieter Gerlich* and Stevan Horning

Fakultät für Physik, Universität Freiburg, D 7800 Freiburg, Germany

Received May 13, 1992 (Revised Manuscript Received August 26, 1992)

Contents

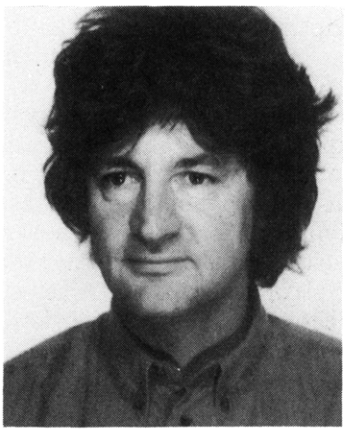

Dieter Gerlich studied physics at the University of Freiburg, where he received his Diplom-Physiker degree in 1971. In 1977 he obtained his doctoral degree under the supervision of Professor Dr. Ch. Schlier with a thesis about reactive proton–hydrogen scattering. After a postdoctorate in Professor Y. T. Lee's laboratory in 1978/79 he worked at the University of Freiburg on ion–molecule reactions developing and using radio frequency ion guides and ion traps. In 1989 he completed his Habilitation in experimental physics. His principle research interests include collision dynamics at very low energies and state-to-state studies of ion–molecule reactions using laser methods.

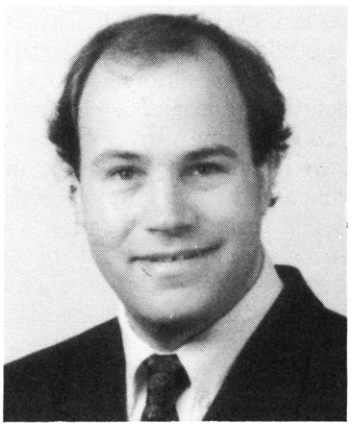

Stevan Horning is a chemist who has spent his career in several areas of mass spectrometry. He was raised in Carmel, CA, and attended the University of California, Los Angeles, where in 1984 he attained his B.S. in Biochemistry. Following a stay with Professor Dr. Donike in Köln, Germany, he joined the research group of Professor R. G. Cooks at Purdue University and in 1990 he received his Ph.D. in Chemistry. Thereafter he was awarded an Alexander von Humboldt Fellowship and has enjoyed the opportunity to spend several profitable months in the laboratory of Dr. D. Gerlich at the University of Freiburg.

I. Introduction

As was originally discussed by Herbst and Klemperer,[1] the low density and low temperature of interstellar regions restricts the gas-phase chemistry to exothermic binary reactions without activation energy. Since most of the neutral reactions are hindered by barriers, ionic gas-phase reactions play a dominant role in the synthesis of interstellar molecules. A summary of the importance of ion–molecule reactions in the chemistry of diffuse and dense interstellar clouds and a nice overview of the different routes to the synthesis of molecules detected in interstellar clouds is given in the review by D. Smith in this thematic issue of *Chemical Reviews*.[2]

Since in some important steps in the synthetic pathways not only neutral reactions but also ion–molecule reactions founder because of their endothermicity or a barrier, several groups suggested in the 1970s the possibility of a radiative association process for overcoming such problems.[1,3–5] One prominent example is the first step in the chain of hydrocarbon chemistry: a collision of C^+ with H_2 cannot lead to $CH^+ + H$ since this reaction requires 0.4 eV, but the strongly bound CH_2^+ excited collision complex can stabilize by the spontaneous emission of a photon. There are many other reaction systems where the intermediate collision complex can be regarded as a highly excited state of a molecule, and it is now generally accepted that radiative association is an important process in the formation of complex molecules in low-density interstellar clouds.[6–8]

0009-2665/92/0792-1509$10.00/0

Due to the importance of this special class of bimolecular reactions, the last decade has witnessed an intense interest in the theory of radiative association processes and several theoretical models have been proposed.[9-11] Most theories utilize statistical approximations and it is commonly assumed that the collision process can be treated in well-defined steps, first complex formation and then radiative stabilization competing with unimolecular decay. The quality of the assumptions and approximations that are made can be partially tested by comparing calculated and measured ternary rate coefficients, and many examples have shown that statistical approaches are rather realistic descriptions of complex formation and decay; however, large errors enter into the prediction of radiative rate coefficients due to uncertainties in the theoretical treatment of the radiative transitions. Several attempts to predict rates for vibrational infrared emission have been reported,[7,12-14] but in general the results provide only order of magnitude estimates. The situation is even worse for those reaction systems where it is unclear whether radiative transitions occur between vibrational levels or low-lying excited electronic states. In the latter case the radiative association rate coefficient can be enhanced, often by a considerable factor.[15]

To characterize experimental methods which provide information related to radiative association rate coefficients, it is useful to distinguish them first according to the accessible density range. High-density experiments such as swarm methods and free jet flow reactors are restricted to the study of ternary association, an important variant of radiative association. At low densities the overall sensitivity is the second criterion used to characterize the available methods. All low-density experiments utilize ion-trapping techniques to accumulate a sufficient number of products. First results on radiative association rate coefficients were obtained with ion cyclotron apparatuses.[12,16] This experimental method was, and still is,[7,17] predominantly used to examine reactions of polyatomic systems, where radiative association rate coefficients are larger than 10^{-10} cm^3/s at room temperature. Since this field has just been reviewed,[18] and since association of aromatic molecules is discussed in the article of Bohme,[19] the present chapter is restricted to radiative association processes involving small systems of astrophysical relevance. The experimental study of these reactions requires low temperatures and a very high sensitivity, and only a few measurements have been reported so far.[20,21]

This review summarizes recent progress made with the rather new but rapidly developing method of temperature-variable radio frequency (rf) ion traps. It is organized as follows. After a few remarks concerning semiempirical and theoretical descriptions of association processes in section II, a brief overview of different experimental methods and a detailed description of the rf ion-trapping technique are given in section III. Section IV presents results for several ion–molecule reactions important in interstellar chemistry which are shown schematically in Figure 1. In addition to reactions of $C_xH_y^+$ ions with H_2 and CO, the two most abundant molecules in interstellar space, the prototype reaction $H^+ + H_2$ is used to illustrate some fundamental concepts. Concluding section VI is a description of new applications of lasers to the study of the radiative association process.

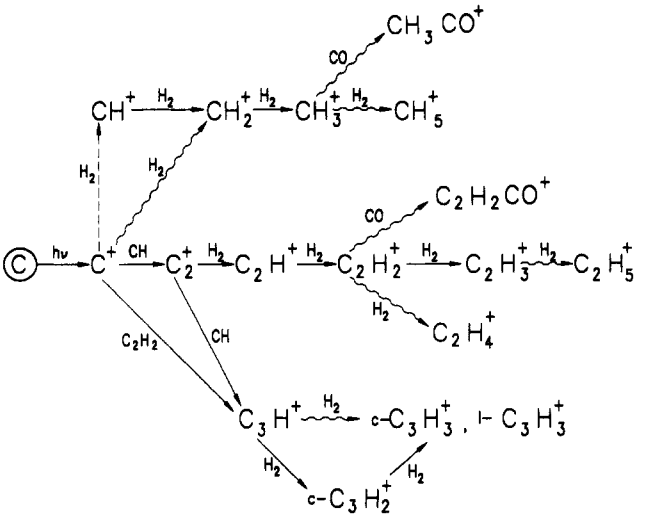

Figure 1. Sample representation of ion chemistry in diffuse interstellar clouds (solid lines indicate fast bimolecular reactions, dashed lines endothermic processes or processes with barriers, and wavy lines radiative association). This figure provides an overview of the series of hydrocarbon reactions which are discussed in this review (for a more complete survey of routes for the synthesis of interstellar molecules see ref 2). For some of the reactions, radiative association rate coefficients have been measured. In the case of $C_3H^+ + H_2$, erroneous conclusions from high-pressure measurements are corrected and discussed. For $C_2H_4^+$ formation via radiative association of $C_2H_2^+$ and H_2, a radiative rate coefficient has been determined, although there are some experimental hints that the bimolecular $C_2H_3^+$ channel may be allowed at very low energies via a tunneling process.

II. Association Reactions: Theoretical Considerations

Due to the importance of radiative association in interstellar chemistry, the last decade has witnessed an intense interest in the theory of these process. Although it is beyond the scope of this review to explain the different theoretical approaches, it is necessary to summarize some of the fundamental assumptions which are used to describe this process. In this reaction two species come together to form an intermediate which is stabilized via the emission of a photon. This is the only association process which occurs at the low densities of interstellar space. Under most experimental conditions, however, the intermediate can also be stabilized by collision with a third body. The overall association reaction

$$A^+ + B \xrightarrow{k^*} AB^+ \qquad (1)$$

is usually described by an apparent second-order rate coefficient, k^*. A rigorous theoretical calculation of this experimentally observable value requires in general a master equation approach accounting for the elementary steps which either contribute to stabilization or compete against it.[22] The following empirical description, commonly used in the evaluation of experimentally determined k^* values,[16] is a rather simple approximation and describes radiative and collisional stabilization and competing pathways using just a few parameters such as mean lifetimes.

Table I. Summary of the Symbols Used To Describe the Elementary Steps of $A^+ + B \rightleftarrows (AB^+)^*$ Complex Formation, Decay, and Stabilization by Emission of a Photon or by a Collision with Target Gas B or with Additional Buffer Gas M

k_c	bimolecular rate coefficient for complex formation
k_L	Langevin rate coefficient for complex formation
k^*	apparent second-order rate coefficient for association
k_T	bimolecular rate coefficient for radiative association
k_3	three-body association rate coefficient
$1/\tau_{dis}$	rate of unimolecular redissociation into reactants
$1/\tau_{rxn}$	rate of unimolecular dissociation into products
$1/\tau_r$	radiative emission rate
$1/\tau_B = k_B[B]$	rate of stabilizing collisions with the molecule B
$1/\tau_M = k_M[M]$	rate of stabilizing collisions with the buffer gas molecule M
f_B	stabilization efficiency factor ($f_B \leq 1$), $k_B = k_L f_B$
f_M	stabilization efficiency factor ($f_M \leq 1$), $k_M = k_L f_M$

In most theoretical descriptions, process 1 is considered to proceed in two independent stages, complex formation and stabilization. In the first step the colliding molecules A^+ and B form a collision complex with a bimolecular rate coefficient k_c:

$$A^+ + B \xrightarrow{k_c} (AB^+)^* \tag{2}$$

The term complex is used to denote a long-lived intermediate molecular ion with a total internal energy above its dissociation limit. Although these states are energetically degenerate with scattering states they are assumed to be metastable (resonances). For most practical purposes it is sufficient to introduce a mean value to describe the complex lifetime:

$$(AB^+)^* \xrightarrow{\tau_{dis}} A^+ + B \tag{3}$$

Under most experimental conditions this back-dissociation process to the reactants dominates, and only a minor fraction of the complexes are stabilized either via emission of a photon

$$(AB^+)^* \xrightarrow{\tau_r} AB^+ + h\nu \tag{4}$$

or by stabilizing collisions with a neutral reactant molecule B

$$(AB^+)^* + B \xrightarrow{\tau_B} AB^+ + B \tag{5}$$

If the experiment is performed with an additional buffer gas M, one also has to account for the stabilization process:

$$(AB^+)^* + M \xrightarrow{\tau_M} AB^+ + M \tag{6}$$

In some cases, the excited intermediate can also decay into reaction products $C^+ + D$ with a rate $1/\tau_{rxn}$:

$$(AB^+)^* \xrightarrow{\tau_{rxn}} C^+ + D \tag{7}$$

An overview of the symbols used and their abbreviations is given in Table I.

With the elementary processes 2–7, the overall formation of stable products AB^+ can be described by the apparent second-order rate coefficient

$$k^* = k_c(1/\tau_M + 1/\tau_B + 1/\tau_r)/(1/\tau_{dis} + 1/\tau_{rxn} + 1/\tau_M + 1/\tau_B + 1/\tau_r) \tag{8}$$

while reaction which occurs with a bimolecular rate coefficient is described using

$$k_{rxn} = k_c(1/\tau_{rxn})/(1/\tau_{dis} + 1/\tau_{rxn} + 1/\tau_M + 1/\tau_B + 1/\tau_r) \tag{9}$$

The collisional stabilization rate with a third body B is written as

$$1/\tau_B = k_B[B] \tag{10}$$

where [B] is the density of the neutral gas and k_B is the rate coefficient for stabilizing $(AB^+)^*$ by collision with B. It is common to compare the rate coefficient k_B with the Langevin rate coefficient, k_L, by introducing the stabilization efficiency factor f_B

$$k_B = k_L f_B \tag{11}$$

By analogy, the same holds for the buffer gas M, whereby the values for f_M may be quite different from f_B, especially for the commonly used buffer gas He. Substituting the eq 10 in eq 8 leads to

$$k^* = k_c(k_M[M] + k_B[B] + 1/\tau_r)/(1/\tau_{dis} + 1/\tau_{rxn} + k_M[M] + k_B[B] + 1/\tau_r) \tag{12}$$

Depending on the experimental conditions, different approximations of eq 12 can be used. Ion-trap experiments are often performed without buffer gas ([M] = 0) and at low densities ([B] → 0). If, in addition, the complex lifetime is very short ($\tau_{dis} \ll \tau_r$) all terms in the denominator with exception of $1/\tau_{dis}$ can be neglected leading to

$$k^* = k_c(\tau_{dis}k_B[B] + \tau_{dis}/\tau_r) \tag{13}$$

Introducing the bimolecular radiative rate coefficient

$$k_r = k_c(\tau_{dis}/\tau_r) \tag{14}$$

and the three-body association rate coefficient

$$k_3 = k_c\tau_{dis}k_B \tag{15}$$

Equation 13 can be written as

$$k^* = k_3[B] + k_r \tag{16}$$

From eqs 14 and 15 one sees immediately that in the low-density limit the radiative lifetime, τ_r, is directly related to the two measured quantities k_3 and k_r, and that the only uncertain parameter is k_B

$$\tau_r = k_3/(k_r k_B) \tag{17}$$

Swarm experiments, on the other hand, are performed using large buffer gas densities [M], and association reactions often proceed near the saturation limit. Assuming

$$k_M[M] \ll 1/\tau_{dis} + 1/\tau_{rxn} + k_B[B] + 1/\tau_r \tag{18}$$

eq 12 reduces to

$$k^* = k_c \tag{19}$$

In many applications it is sufficient to first obtain an estimate of k_c based on simple model assumptions. In order to determine the bimolecular rate coefficient for complex formation and complex stabilization, k_c and k_M respectively, it is common to use capture theories

that only consider the long-range electrostatic potential resulting in the Langevin rate coefficient for nonpolar molecules. As a typical value for a collision between a hydrocarbon ion and hydrogen (reduced mass $\mu \sim 2$, polarizability $\alpha_{H_2} = 0.79$ Å^3) one obtains

$$k_L = 1.47 \times 10^{-9}\ \mathrm{cm^3/s} \qquad (20)$$

There are several examples where the complex formation rate, k_c, is significantly smaller than k_L. This can be due to the participation of several potential surfaces which are degenerate at large distance but some of which become repulsive at lower distances.[23] Steric factors or anisotropic potentials can also lead to deviations from the simple polarization model. Another explanation for $k_c \ll k_L$ may be the formation of weakly bound complexes in a first step most of which rapidly decay back into reactants with exception of a small fraction which undergoes conversion into long-lived intermediates.[24]

An important factor in this semiempirical description is the stabilization efficiency f. Commonly used values of f range from 0.5 to 0.1, and in this review $f = 0.2$ is always used unless otherwise stated. On the basis of simple statistical arguments, molecules are expected to be more efficient stabilizers than atoms. In the process described in eq 5 the stabilized product AB^+ can also be formed by a switching process[25] which may lead to a larger stabilization efficiency. In most of the examples presented in section IV, hydrogen is shown to be twice as efficient as helium. As an exception it will be shown in section IV.A that H_2 is less efficient than He for stabilization of the $H^+ \cdot H_2$ complex. For comparison of stabilization rates for H_2 or He ($\alpha_{He} = 0.21$ Å^3) one must account for the fact that the collision rate with He is about a factor 2.75 smaller:

$$k_L(\alpha_{He}, \mu = 4) = k_L(\alpha_{H_2}, \mu = 2)/2.75 \qquad (21)$$

So far in this semiempirical description, the intermediate complex has been described using only a single value for each of the parameters τ_{dis}, τ_{rxn}, τ_M, etc., each of which is assumed to only be a function of the total energy E. In reality, however, these parameters may depend significantly on other conserved quantum numbers such as the total angular momentum J and parity, or on quantum numbers which are approximately conserved during the lifetime of the complex due to dynamical constraints such as the total nuclear spin. This leads, for example, to (E, J, ...)-dependent lifetimes, reaction probabilities, etc. Therefore it is sometimes reasonable or even necessary, as will be shown in section IV, to evaluate experimental data using more parameters. Simple extensions of the model described above are obtained by introducing two distinct complexes 1 and 2. Such a model has been proposed for example in the $C_3H^+ + H_2$ reaction,[24] where it was assumed that a short-lived and a long-lived complex, which are connected via a barrier, are populated in sequential steps. The simple two-complex model used in this paper, is based on the assumption that different initial conditions (e.g. orbital angular momentum, orientation, etc.) lead to a branching between the two complexes. If there is no conversion between the two classes of complexes (e.g. due to conversion of quantum numbers or high steric barriers), the apparent second-order rate coefficient can be expressed simply with pairs of parameters, k_{c1}, k_{c2}, τ_{dis1}, τ_{dis2}, etc.

$$k^* = k_{c1}(k_M[M] + k_B[B] + 1/\tau_r)/(1/\tau_{dis1} + k_M[M] + k_B[B] + 1/\tau_r) + k_{c2}(k_M[M] + k_B[B] + 1/\tau_r)/(1/\tau_{dis2} + k_M[M] + k_B[B] + 1/\tau_r) \qquad (22)$$

If the two complex lifetimes or the two complex formation rate coefficients are largely different, several density-dependent approximations can be derived from this equation. For $\tau_{dis2} \gg \tau_{dis1}$, saturation of the second complex will occur at much lower densities than for the short-lived one. As seen in some examples in section IV, the rate coefficient for formation of the short-lived complex, k_{c1}, is significantly larger than k_{c2}, and hence the high density limit is dominated by complex 1, viz.

$$k^* = k_{c1} \qquad (23)$$

Nonetheless, the low density limit of k^* can be determined for complex 2

$$k^* = k_{c2}(\tau_{dis2}/\tau_r) \qquad (24)$$

provided that the product $\tau_{dis2}k_{c2}$ is larger than $\tau_{dis1}k_{c1}$. This situation is discussed in greater detail in sections IV.D and IV.F. Simple extensions of the model described by eq 22 (e.g. the introduction of different stabilization efficiencies for the two complexes, the formation of three separate complexes, etc.) are straightforward. The inclusion of an additional reaction channel will be discussed in section IV.E. Also the construction of more complicated models such as a network of several complexes with a variety of couplings and the solution of the adequate master equations pose no principle problems; however, they should be motivated from ab initio studies.

In the preceding model, the ternary and radiative association processes were described using purely empirical parameters, k_c, τ_{dis}, and τ_r. As was already discussed, theoretical predictions for the complex formation rate, k_c, are usually based on simple capture models. In the following, additional remarks about theoretical models, especially those used to calculate the two time constants, τ_{dis} and τ_r, are made. In all current theories, statistical approximations are used and the most rigorous approach to describe complex formation and decay, which satisfies microscopic reversibility and conserves total angular momentum, is the phase-space theory.[9,26,27] Worthy of note in this context is the generalized statistical approximation derived from Feshbach's formulation of resonance scattering[28] and the detailed prescription on how to include symmetry selection rules in statistical theories.[29] The correct treatment of nuclear spin statistics in statistical models is especially important for collisions of hydrogen-containing ions with o- and p-hydrogen[30] and is still under debate.[31]

The majority of the estimates of complex decay rates reported in the literature is based on simplified statistical approximations and most complex lifetimes are derived from RRKM-like approaches using the density of states in the intermediate complex and in the "transition state". These semiquantitative descriptions have the advantage that general features for a certain class of molecules, e.g. hydrocarbons,[7,8] can be predicted and that general rules can be derived for the

dependence of the lifetimes on the binding energy or complexity of the system. Of special significance for the interpretation of these results and for the inter- or extrapolation of measured rate coefficients is the inverse dependence on temperature of the three-body association reaction rate coefficients. The modified thermal treatment developed by Bates[10] and Herbst[11] predicts that the rate coefficient for ternary association should vary as

$$k_3 \sim \tau_{dis} \sim T^{-(l/2+\delta)} \qquad (25)$$

where l is the number of rotational degrees of freedom in the separated reactants and δ is used to account for the temperature dependence of the stabilization efficiency f. At high temperatures, vibrational excitation has to be included, while at very low temperatures the density of states in the transition state becomes very small and finally even the rotational degrees of freedom become frozen. It can be presumed that the radiative association rate coefficient possesses the same dependence on temperature since the radiation process is predominantly determined by the well depth of the intermediate molecule which, at the temperatures of interest, is much larger than the small collision energy.

A satisfying theoretical treatment of the radiation process from the collision complex is not yet available and most of the predicted radiative lifetimes are very unreliable. Problems arise from the uncertainty of how to describe the complex which must be regarded as a molecular system of extremely high energy content and high complexity and which is coupled to the dissociation limit. The situation becomes even more complicated if different electronic potential surfaces are involved, and it may happen that the radiative lifetime for only slightly different complexes differs by orders of magnitude if one of them can radiate via an electronic rather than a vibrational transition. Note however, that the radiative rate coefficient is also determined by the complex lifetime (eq 14) and that the lower state density on an electronically excited potential surface reduces the complex lifetime.[15]

In certain cases, it may be a good approximation to assume that the energy is localized in well-characterized states (normal modes, local modes, or other suitable basis sets) and in this case simple descriptions used for low-level excitations (states, molecular constants) are applicable. For polyatomic molecules, several estimation schemes have been reported for order of magnitude predictions,[7,14] accounting for typical IR-active modes of the intermediate complex.

In other cases complete energy scrambling may prevail due to complicated dynamical coupling of molecular states, and the spectroscopic descriptions of these systems require new concepts. One approach for the characterization of the highly excited systems is based on the numerical integration of the classical equation of motion on potential surfaces. Provided that also the surface of the dipole moment μ is known, the trajectories can be related to a spectral density by means of the dipole correlation function. Most of this kind of work has been performed so far on artificial two-dimensional model systems. More related remarks and applications to the $H^+ + H_2$ system are found in section IV.A.

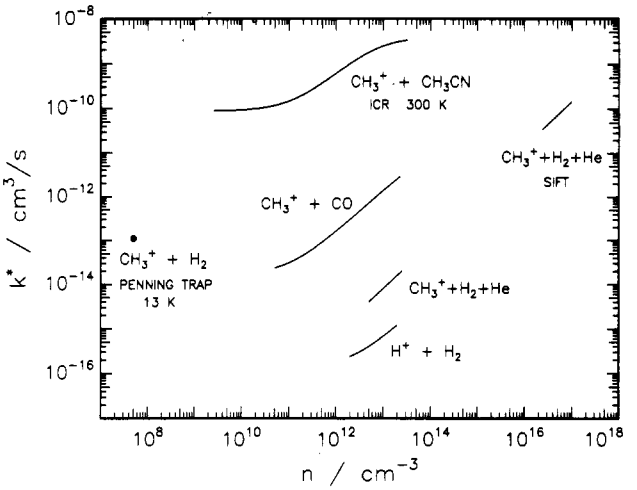

Figure 2. Comparison of association reaction rate coefficients for various systems, measured using different techniques and at very different densities (80 K unless otherwise indicated). Plotted are the apparent second-order rate coefficients as a function of target density. The uppermost curve shows association of $CH_3^+ + CH_3CN$ studied in an ICR cell.[16] This reaction is a typical example of a complex with an extremely long lifetime. The data below 10^{10} cm^{-3} indicate radiative association with $k_r = 10^{-10}$ cm^3/s, saturation effects become dominant above 10^{13} cm^{-3}. The other examples will be discussed in section IV and are plotted here primarily to indicate qualitatively the dependence of k^* on the number of degrees of freedom. The $CH_3^+ + H_2 + He$ association process has been studied in the 10^{13}-cm^{-3} range in an rf ion trap[21] and above 10^{16} cm^3 in a SIFT apparatus.[32] The determined ternary rate coefficients are in good agreement. The solid circle at very low densities represents the radiative association rate coefficient measured in a Penning ion trap.[20]

III. Experimental Methods

Upon initial inspection of the discussion in section II, the ideal experiment for measuring exclusively radiative association rate coefficients for astrophysical applications is one which most closely resembles the conditions found in interstellar clouds. An advantage of such a low-temperature experiment would be that complexes with very long lifetimes are formed (see eq 25) and one could expect that the radiative association rate reaches its maximum. Moreover, the low-density conditions ensure that stabilization via ternary collisions need not be considered as a competing process. The actual experiment, however, is limited by several practical considerations. Although very low densities can be attained experimentally, the probability of observing a single reaction product increases proportionally to the density. In addition, in most experiments, a sufficiently large number of nonreactive collisions is necessary to assure thermalization of the ion. Therefore, one has to compromise in choosing the optimal density for accurately measuring radiative association rate coefficients. In general this optimum will be in a region where radiative processes and ternary association processes create a comparable number of stabilized products, i.e. where the relationship $n \sim k_r/k_3$ holds. Some of these ideas are illustrated in Figure 2, which shows effective rate coefficients as a function of the density for a few reaction systems. For the $H^+ + H_2$ collision system, the optimum density is in the 10^{12}-cm^{-3} range, while for the $CH_3^+ + CH_3CN$ system it is in the 10^{10}-cm^{-3} range, as can be seen from the

curvature of the apparent second-order rate coefficient (see eq 16).

To gain insight into the separate steps determining the radiative association process the experiment has to cover a wide density range, usually not accessible with a single method. A direct determination of the complex formation rate coefficient, k_c, is only possible at densities where saturation occurs. As illustrated in Figure 2, this can occur at rather low densities as in the $CH_3^+ + CH_3CN$ example. In other cases, densities above 10^{16} cm^{-3} are required. Based on assumptions of the collisional stabilization efficiency, the onset of saturation determines the complex lifetime (see eq 15). The situation becomes more complicated if the concept of a single mean lifetime is not adequate and if, for example, two classes of complexes are formed with very distinct lifetimes (eq 22). To reveal early saturation effects caused by the long-lived class, a variation of the target gas density over a wide range is required as will be seen in several examples in section IV. Another important parameter fundamental to the understanding of the radiative association process is the radiative lifetime. According to eq 17 this value can be directly derived from two measured quantities, k_3 and k_r. Provided that both rate coefficients have been measured under identical experimental conditions, the only uncertainty in τ_r is the stabilization efficiency.

In the remainder of this section, ion-swarm and ion-trap experiments which are used to measure radiative and ternary association rate coefficients are presented. These experiments are discussed based on criteria such as the density and temperature range, the method of ion preparation and thermalization, and also the interaction time which determines the sensitivity. In section III.B, rf ion traps and principles of ion storage in inhomogeneous rf fields are discussed. Finally, in section III.C measuring procedures and several experimental tests of rf ion storage devices are presented.

A. Overview of Different Techniques

Flowing afterglow and selected-ion flow tube (SIFT) techniques have provided a large body of kinetic and thermodynamic data for reactions of hydrocarbon ions with a variety of neutral species.[32,33] The short time interval between collisions, typically 0.1 μs, in these high density, temperature-variable experiments ensure thermalization of the ions; however, these methods do not allow direct measurement of radiative association rate coefficients. Instead, as discussed in section II, collision complex lifetimes are used to indirectly determine radiative association rate coefficients. Ternary association rate coefficients are measured by recording the change in the effective rate coefficient as a function of He gas density.[32] In many cases the effective rate coefficient increases proportionally to the density as shown in Figure 2 for $CH_3^+ + H_2 + He$ ternary association. In other cases, no change in the effective rate coefficient is observed and this is attributed to saturation of the collision complex, i.e. the time between collisions is much shorter than the complex lifetime and all complexes formed are stabilized. This is especially problematic at lower temperatures where complex lifetimes are significantly long. Temperatures below 80 K have been attained using a drift tube cooled with liquid helium.[34] This apparatus has been used to study the ternary association reaction of He^+ with He, as discussed in section III.C.

An experimental limitation at low temperatures is condensation of the neutral species. To examine association reactions at low temperatures with condensable gases, supersonic expansion methods must be used. One example is the Cinétique de Réaction en Ecoulements Supersoniques Uniformes (CRESU) technique[35] where ions of a selected mass are injected into the core of a several centimeter thick supersonic flow of He containing a small amount of the neutral molecules of interest. This technique has been used, for example, to study the ternary association of CH_3^+ with H_2 and CO. An interesting feature of these data is that for reactions with H_2 at temperatures below 80 K a departure from the power law given in eq 25 was reported.

An extension to temperatures below 3 K has been made possible by the development of the free jet flow reactor.[36] In this experiment, a free jet expansion of a mixture of H_2 seeded with a given species, e.g. C_2H_2, is formed by an expansion through a 0.1-mm nozzle orifice. At a variable distance from the nozzle, the neutral species is selectively ionized either by resonance-enhanced multiphoton ionization or by one-photon vacuum ultraviolet ionization. The ion packet flows and collides with the abundant H_2 gas jet along a field free path, and at a given distance the reactant and product ions are extracted and analyzed by their time of flight. A large number of bimolecular and ternary ion–molecule reactions have been examined using this technique.[37] Reactions of $C_2H_2^+$ with H_2 at ultra-low temperatures leading to the formation of $C_2H_3^+$ and $C_2H_4^+$ are discussed in section IV.D.

The variety of methods described has been used to study a large number of ion–molecule reactions over a wide range of densities and temperatures, mostly under thermal conditions. Although not mentioned in the preceding discussion, an inherent limitation of these techniques is that the interaction time is determined by the drift or flight time. In the supersonic expansions this time is usually below 100 μs, and this sets an experimental limit on the minimum reaction rate coefficient which can be measured. To achieve much longer interaction times the ions must be stored in a trapping device. Several ion-trap devices which have been used to study association reactions are discussed here and in section III.B.

The most common ion storage technique used to study radiative and ternary association reactions is the ion cyclotron resonance (ICR) apparatus. In this device ions can be trapped for very long times, and with the use of a buffer gas thermal conditions can be attained. Most association studies performed thus far have focused on polyatomic heteroatom systems which undergo rapid radiative and ternary association reaction at room temperature.[7,16] Although these reactions are not discussed in this review, their interstellar relevance has been discussed recently in ref 38.

In an ICR apparatus the pressure can be varied over a wide range, typically between 10^{-8} and 10^{-4} Torr, and direct information on the radiative and ternary association reactions can be obtained as illustrated in Figure 2. Several ternary rate coefficients have been determined for reactions which are otherwise too rapid to be

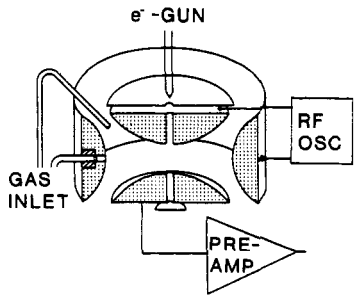

Figure 3. Schematic diagram of the cooled (13 K) Penning ion trap.[39] Indicated are the electron gun for in situ ion generation, the precooled gas inlet, the resonance circuit for mass selective heating or ejection, and the preamplifier for nondestructive detection of the ion cloud.

measured in SIFT experiments.[16] A distinct advantage of this low density method is that the time between collisions is sufficiently long, on the order of 0.1 to 100 ms, that information on radiative processes can be derived. In some cases, it has been possible to directly measure complex lifetimes on the order of several microseconds[17] and to determine radiative lifetimes of several milliseconds.[7]

Storage of ions in magnetic fields at very low temperatures has been achieved using a liquid helium cooled Penning trap apparatus depicted in Figure 3. With this device the first direct measurement of radiative association at very low temperatures was performed by Barlow, Dunn, and Schauer.[20,39] Results for reactions of C^+ and CH_3^+ with H_2 using this apparatus are presented in sections IV.B and IV.C, respectively. In this experiment ions are initially cooled by collisions with 10 K normal-H_2 at a density on the order of 10^7 cm^{-3} (see Figure 2) which requires many minutes. The primary and product ions are monitored by mass-selective excitation of the ion cyclotron motion and measuring the ion image current. With this nondestructive detection scheme it is possible to study the reactivity of a single-ion sample for a period of hours. A difficulty in this experiment is the determination of the H_2 density and the ion internal temperature. Some of the uncertainties are due to the use of normal-H_2 and heating collisions with $H_2(j = 1)$. The sensitivity of the apparatus allows rate coefficients on the order of 10^{-15} cm^3/s to be determined.

Rf quadrupole ion traps have also been used by a large number of investigators to examine ion–molecule reactions.[40,41] This device, however, is poorly suited for studying low-energy association processes due to rf heating of the stored ions. This heating process can be avoided by using higher order field geometries as discussed in the following sections.

B. Radio Frequency Ion Traps

Several radio frequency ion-trap devices have been developed for examining ion–molecule association processes over a very wide range of temperatures. The characteristic features of these ion traps will be discussed below. The ion-trap device is integrated into an ion-beam apparatus shown schematically in Figure 4. The individual elements of this apparatus (radio frequency storage ion source, quadrupole ion guides, etc.) have been described in ref 42. Primary ions, created by electron bombardment and prethermalized in the high-pressure storage ion source, are selected according to their mass and energy and injected into the ion trap. Usually, the primary ions are selected by operating the quadrupole in the low pass mass filter mode,[42] avoiding rf heating of the kinetic energy of the ions. Upon entering the ion trap, the ions undergo many collisions with the target gas or additional buffer gas, usually He, thereby adapting the temperature of the trap environment. After a given reaction time (microseconds to minutes), the primary and product ions are extracted from the trap, mass analyzed, and detected with a scintillation detector. The apparatus is optically transparent in the axial direction to facilitate the combination of laser methods with the storage ion trap.

The fundamental principles of ion confinement in inhomogeneous radio frequency fields have recently been discussed in detail in ref 42, and therefore only a very short presentation is given here. The motion of an ion with charge q and mass m in an electrical inhomogeneous rf field, $\mathbf{E}_0 \cos \Omega t$, can be described as a rapidly oscillating motion superimposed on a smooth trajectory. At sufficiently high frequencies the smooth trajectory can be derived from a time independent *effective potential*:[43-45]

$$V^* = q^2\mathbf{E}_0^2/4m\Omega^2 \tag{26}$$

The range of validity of this adiabatic approximation can be estimated with the *adiabaticity parameter*:

$$\eta(r) = 2q|\nabla E_0|/m\Omega^2 \tag{27}$$

For most applications, the two functions V^* and η allow a satisfying characterization of the properties of arbitrary field geometries and, as a rule of thumb, safe operation within the validity of the adiabatic approximation is guaranteed if the parameter η remain smaller than 0.3 along the ion trajectory.[42]

Under such conditions the total energy is an adiabatic constant of the motion. Nonetheless, the rf field has a temporary influence on the ion energy and, as discussed in detail in ref 42, the time-averaged energy distribution of stored ions becomes very narrow only if one chooses a field geometry with a wide field-free region. A very simple geometry which fulfills this condition uses rotationally symmetric boundary conditions. A first realization, a trap made from metal plates with circular holes, was developed by Teloy and Bahr.[46] Two recently developed versions of cooled ring-electrode traps are described below. Another important class of electrode systems are the two-dimensional multipoles.

The effective potential and the η parameter have been discussed for different geometries in ref 42, and here only the equations for the $2n$-poles are briefly mentioned. Introducing the characteristic energy[47]

$$\epsilon = (1/2n^2)m\Omega^2 r_0^2 \tag{28}$$

which combines the parameters mass, frequency, and the inscribed radius r_0 of the multipole arrangement, and denoting by V_0 the amplitude of the rf voltage applied to the electrodes, the effective potential and the stability parameter can be expressed as

$$V^*(r) = \frac{1}{8}\frac{(qV_0)^2}{\epsilon}\left(\frac{r}{r_0}\right)^{2n-2} \tag{29}$$

and

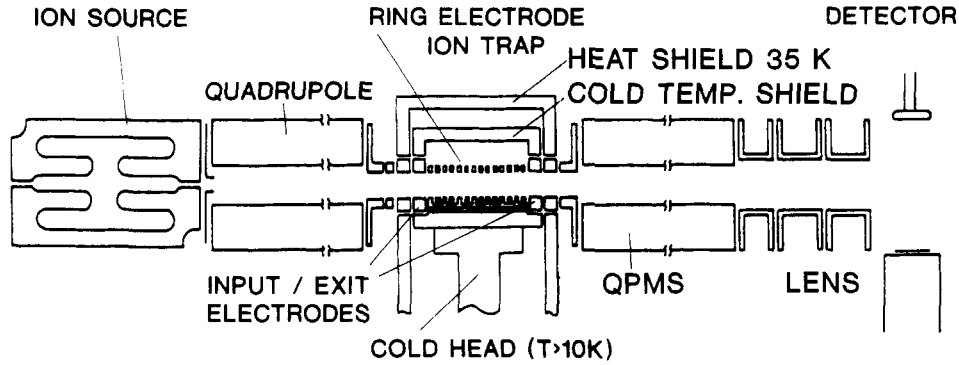

Figure 4. Schematic diagram of the radio frequency ion-trap apparatus. Ions are created by electron bombardment and prethermalized in the storage ion source. The first quadrupole is used either as a mass analyzer or a low-pass mass filter, depending on whether high mass resolution or a narrow energy distribution is required. The temperature-variable ion trap is contained in the center of the apparatus. The entrance and exit electrodes are operated in a pulsed mode for ion injection and extraction, respectively. A quadrupole mass spectrometer is used to analyze the trap contents, and the ions are detected using a scintillation detector. For laser experiments, the apparatus is transparent in the axial direction.

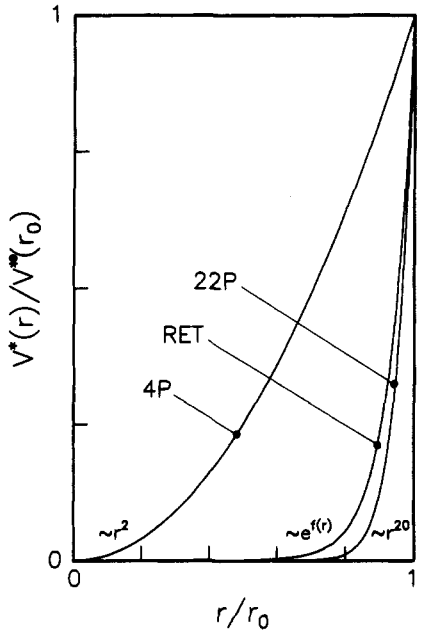

Figure 5. Relative effective potentials $V^*(r)/V^*(r_0)$ as a function of the distance from the center line. The quadrupole (4P) potential is harmonic, in the 22-pole arrangement (22P) the potential increases with the 20th power toward the walls, and in the ring-electrode trap (RET) exponentially (for the geometry, described in Figure 7, $V^* \sim r_0/r \exp[5\pi(r/r_0-1)]$). The wide field-free region of the high-order arrangements leads to the confinement of nearly unperturbed ions.

$$\eta(r) = \frac{n-1}{n}\frac{qV_0}{\epsilon}\left(\frac{r}{r_0}\right)^{n-2} \qquad (30)$$

In the 22-pole ion trap (n = 11, r_0 = 0.5 cm) which is described below, typical operating conditions for the storage of $C_2H_2^+$ ions are V_0 = 50 V and $\Omega = 2\pi$ 16 MHz. From these parameters one obtains ϵ = 281 eV, an effective potential of $V^*(r = r_0)$ = 1.1 eV and $\eta(r = r_0)$ = 0.16.

The r dependence of the effective potential for three-electrode arrangements are compared in Figure 5. With the geometries used (see below) the effective potential of the 22-pole, which is proportional to r^{20} increases even steeper than that of the ring electrode trap. In both cases, however, one obtains a wide field-free region in contrast to the harmonic effective potential of the rf quadrupole.

To aid in the interpretation of experiments employing ions stored in inhomogeneous rf fields in the presence of a cold buffer gas, it is necessary to understand the distortion of the ion kinetic energy distribution caused by the confining rf field. If the trapping volume is distinguished by a wide, flat potential with very steep repulsive walls, most collisions with the buffer gas occur in the field-free region leading to a rather fast adaption of the ion energy distribution to the thermal distribution of the neutrals. The few collisions occurring in regions of higher field cause the ion mean energy to be slightly higher than that of the ambient gas.

Quantitative estimates of the energy distributions of stored ions have been calculated by numerical integration of the equation of motion, and including a realistic model for collisions with neutral gas.[42,48] Some of the results are plotted in Figure 6 in a presentation which allows one to simultaneously view the low- and the high-energy regimes, although the logarithmic energy scale can lead to a somewhat erroneous visual weighting of the area normalized distributions. In the two depicted examples, H^+ and C^+ ions are stored in a ring electrode trap (r_0 = 0.5 cm) with 80 K normal-H_2. An analysis of the H^+ distribution, plotted in the upper panel, indicates that 75% of the H^+ ions can be described by a 80 K thermal distribution. An additional 25%, however, resides in a 200 K hot tail. This heating is partly caused by a too low rf frequency (27 MHz) and by the unfavorable mass ratio (light ion in a heavier buffer gas). Both effects are significantly reduced if one goes under otherwise identical conditions to a heavier ion, as shown in the lower panel for C^+. To account for the small fraction of fast ions in this distribution, only a 160 K Maxwell distribution with a relative weight of 10% is needed. An energy distribution of ions stored in a linear quadrupole trap is also compared quantitatively in this figure. Since in such a trap the ions are under the influence of the rf field for a much longer time, the energy distribution becomes significantly broader. In the example shown, more than 50% of the ions stored in the quadrupole are characterized by a temperature of 300 K.

These two examples show that for collisional ion cooling, the rf frequency, the mass ratio, and the trap geometry play an important role. The frequency should be as high as possible, the buffer gas light relative to the ion mass, and the rf trap should have a wide field-

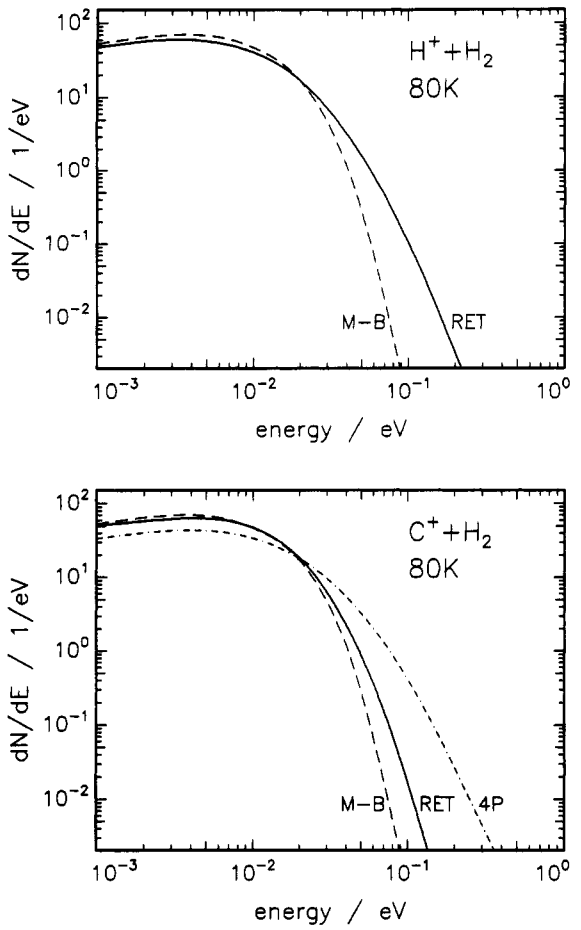

Figure 6. Log/log representation of numerically determined energy distributions for H^+ (upper panel) and C^+ ions (lower panel) stored in a ring-electrode trap (RET) with 80 K H_2 buffer gas. Comparison with the 80 K Maxwell–Boltzmann (M-B) distribution and with the quadrupole trap (4P) distribution shows that the rf field causes some heating; quantitative details are discussed in the text.

free region with steep confining walls, e.g. quadrupole ion traps should be avoided. Finally, it should be noted that it is also important to avoid space charge effects and therefore most rf ion trap experiments have been performed with less than 10^3 ions/cm^3.

Two actual realizations of ion traps are depicted in Figure 7. They consist in both cases of equally spaced electrodes which are alternately connected to the two phases of an rf generator. The ring-electrode device in the upper panel is constructed from 1-mm-thick rings with 10-mm-diameter holes arranged as indicated in Figure 4. The 22-pole depicted in the lower panel of Figure 7, is made from 22 1-mm rods equally spaced on an inscribed radius r_0 = 5 mm. One of the major obstacles in the construction of these devices is the dissipation of rf power which heats the electrodes.[49] In one of the first cooled ring-electrode ion traps,[21,48] this problem was overcome by cooling the device directly by running liquid nitrogen through the stainless steel ring holders and rf coil. The maximum achievable storage time in this trap is limited only by the extent of reactive processes, i.e. reaction with trace impurities, and at 80 K ions can be stored for several minutes with no loss. A few tests demonstrating the capabilities of this device are presented in the following section. The high sensitivity of the apparatus has allowed measurements of reaction rate coefficients as slow as 10^{-16} cm^3/

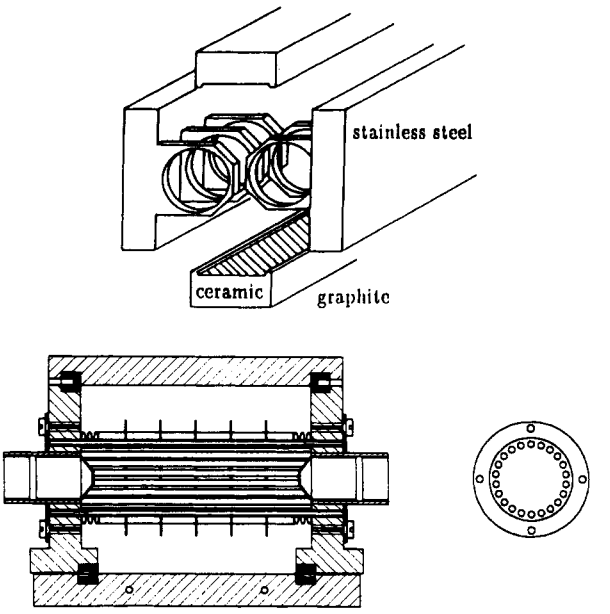

Figure 7. Illustration of two rf ion traps. In the ring-electrode trap shown above the solid holders are cooled directly with liquid nitrogen. In the trap shown below the ions are confined in the rf field of a 22-pole. The entire system is mounted on the cold head of a liquid helium cryocooler. Typical dimensions in both cases are diameter of the storage region, 10 mm, and distance between neighboring electrodes, 2 mm. The two graphite-coated ceramic covers (hatched area in the upper panel) and the additional electrodes (five thin rings in the lower panel) are used for potential corrections in the axial direction.

s, and this trap has proved to be very reliable based on the results of a large number of experiments.[42] The only limitation is that temperatures below 80 K are not accessible.

To extend the operating range to temperatures below 80 K, a ring-electrode trap constructed from copper has been developed which is mounted directly onto the cold head of a liquid helium refrigeration system.[42,50] This trap is integrated into the apparatus shown in Figure 4. A thin sheet of heat-conducting material (Denka, BFG 29) is used to provide electrical insulation and thermal contact between the ≥10 K cold head of the cooling system and the ion trap. This material, however, is not well suited for ultra-high vacuum conditions and reliable measurements using this trap can only be made at temperatures below 50 K. The trap is surrounded by a 35 K heat shield which is connected to the first stage of the cryocooler. All connections to the trap, including the gas inlets and the wires to the rf coil are also precooled to this temperature. At very low temperatures the attainable reagent density is limited by its vapor pressure. For this reason in experiments employing H_2, the temperature is maintained above 15 K to prevent condensation.

Very recently a first version of the 22-pole ion-trap device, shown in the lower panel of Figure 7, has been integrated onto the cold head of a liquid helium refrigerator. Using a different design for the thermal coupling and electrical insulation more suitable vacuum conditions could be achieved. In addition to this and to the already discussed very steep effective potential, this device has several advantages compared to the ring-electrode trap. The axial geometry leads to reduced potential distortions along the axis of the trap, caused

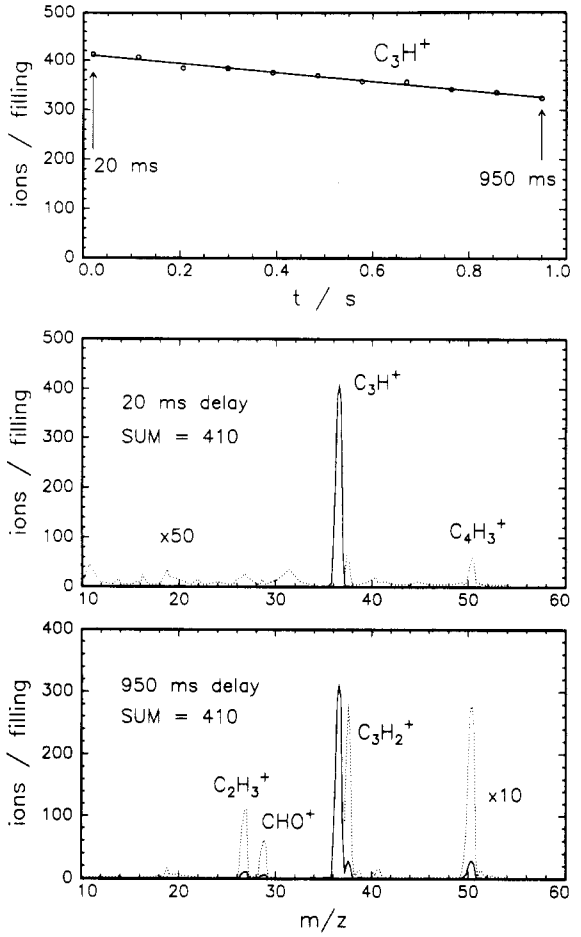

Figure 8. Long-time storage of C_3H^+ ions in He buffer gas (density 2×10^{13} cm^{-3}) at 400 K in the ring-electrode trap. The time constant for the loss of C_3H^+ ions indicated in the upper panel is $\tau = 4.1$ s. This loss is due to reactions with background gases (predominantly H_2O and C_3H_4 from the ion source) as can be seen from the two mass spectra recorded at 20 ms (middle panel) and 950 ms (lowest panel) storage times. Note that the sum of all ions remains constant. From the known rate coefficients[51] of the reactions involved the densities can be estimated, e.g. $[H_2O] \sim 10^{10}$ cm^{-3}.

by surface potential variations, and it has been demonstrated that an ion beam with an axial energy of 1 meV can be trapped. A set of five thin correction electrodes (see Figure 7) can be used to create a shallow potential well in the axial direction to ensure that the ions are located in the center of the trap where the pressure is determined. It is also planned to modulate the voltage applied to these electrodes in an adequate way for mass-selective ion ejection. Another improvement of the apparatus is the integration of two pulsed gas inlets which can be used to inject first the gas used for thermalization and, following a delay, that for reaction.

C. Measuring Procedures and Experimental Tests

An example illustrating the storage capability of the ring electrode ion trap is shown in Figure 8. The number of C_3H^+ ions stored in He buffer gas at 400 K for times up to 1 s decreases slowly due to fast bimolecular reactions with trace amounts of background gases, in this case, methylacetylene (from the ion source) and water. The mass spectra recorded at storage times of

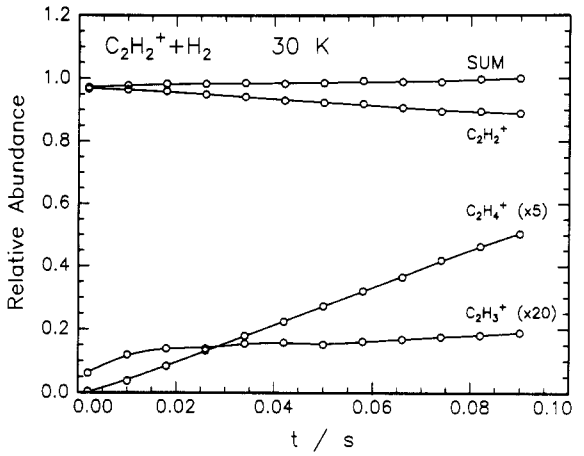

Figure 9. Reaction of $C_2H_2^+$ ions with H_2 (density 3×10^{12} cm^{-3}) in a He buffer gas (density 2×10^{14} cm^{-3}) examined in the 22-pole ion trap at 30 K. Rate coefficients are determined from the time dependence of the primary and product ion abundances. $C_2H_4^+$ association is the dominant reaction while the bimolecular $C_2H_3^+$ product is formed at a significant rate only during the thermalization process within the first 20 ms. Details of the results are discussed in section IV.D.

20 and 950 ms indicate that the total number of ions in the trap remains constant. From the measured increase in the HCO^+ ion at different storage times, the density of H_2O can be determined, $n \sim 10^{10}$ cm^{-3}, using the known rate coefficient. At 80 K the decrease in the C_3H^+ signal is much smaller due to additional cryopumping which largely reduces the density of background gases. The reaction of C_3H^+ with H_2 at 80 K, which leads to the formation of $C_3H_2^+$ and $C_3H_3^+$, is the subject of section IV.E.

Typically, to determine a reaction rate coefficient, the loss in the number of primary ions and the corresponding increase in the number of product ions is monitored as a function of reaction time. Reaction of $C_2H_2^+$ with H_2 in He buffer gas at 30 K leads primarily to the production of $C_2H_4^+$, as depicted in Figure 9. The $C_2H_2^+$ ions were generated by electron bombardment of acetylene and injected with an energy of typically 100 meV into the 22-pole ion trap. In the ion-trap experiment a maximum number of a few hundred primary ions is injected to avoid space charge problems and dead time in the counting system. Initially, a fraction of the $C_2H_2^+$ ions reacts with H_2 to produce $C_2H_3^+$. The fact that this reaction channel rapidly levels off at longer storage times indicates that it is due to internally exited $C_2H_2^+$ ions. After a sufficient number of collisions this reaction proceeds only at very low rate. Determination of the rate coefficient, which is smaller than 5×10^{-14} cm^3/s, is complicated by the large $C_2H_3^+$ background. This background could be avoided by introducing the H_2 reactant with a pulsed gas inlet long after the ions have undergone a large number of thermalizing collisions with the He buffer gas.

The association reaction of CH_3^+ with H_2 varies significantly with temperature, as evidenced by the differences in CH_5^+ production at 45, 65, and 90 K in Figure 10. Note however, that the large change in the measured rate for formation of CH_5^+ is not only due to the temperature dependence of the rate coefficient for this reaction, but also to the temperature dependence of the density of the hydrogen, which is leaked into the

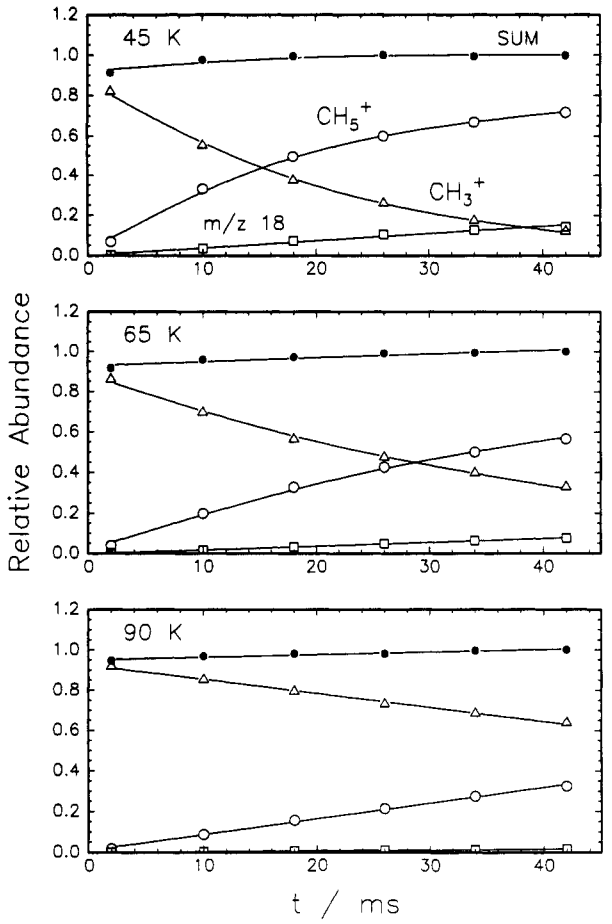

Figure 10. Reaction of CH_3^+ ions with H_2 measured in the 22-pole ion trap at three different temperatures. The dominant process is the formation of the CH_5^+ association product. Also of interest is the production of ions with mass 18 u, indicating reactions with D admixtures or the presence of $^{13}CH_2^+$ isotopes in the primary ions.

22-pole with a constant flow. This is discussed in more detail below.

Reaction rate coefficients are determined by fitting the parameters of an appropriate rate equation to the measured temporal change of the ion composition. For a binary system, such as the reaction $C_2H_2^+ + H_2 \rightarrow C_2H_3^+ + H$ depicted in Figure 9, the attenuation of the primary ion is expressed as

$$dN_1/dt = -knN_1(t) \tag{31}$$

i.e. the number of primary ions, N_1, decreases exponentially with a time constant

$$\tau = (kn)^{-1} \tag{32}$$

where k is the bimolecular or apparent second-order rate coefficient and n the target density. The time constant for the increase in the number of product ions, $N_2(t)$, is expressed in an identical manner. When the rate of product increase is small with respect to the primary intensity, the rate coefficient can be determined from the increase of products, ΔN_2, the time interval, Δt, and the density using the linearized form

$$k^* = \frac{\Delta N_2}{N_1}\frac{1}{n\Delta t} \tag{33}$$

This approximation was used, for example, to determine the rate coefficient for $C_2H_3^+$ formation, by examining the change in $C_2H_3^+$ intensity at storage times between 60 and 80 ms.

The actual density of the neutral species in the ion trap is a function of the gas flow, the trap geometry, the pumping efficiency, and the temperature. At densities below 10^{11} cm^{-3}, n is determined using tabulated reaction rate coefficients,[51] e.g. the reaction $Ar^+ + H_2 \rightarrow ArH^+ + H$. At higher densities, a Leybold VISCOVAC VM 210 vacuum gauge, calibrated with a quoted accuracy of 5%, is used. The gauge itself operates at room temperature and the density in the trap is calculated from the indicated pressure p (millibar) and the trap temperature T (Kelvin) using the relation

$$n = (4.19 \times 10^{17})pT^{-1/2}\ \text{cm}^{-3} \tag{34}$$

This equation holds for molecular flow conditions which always exist at densities below 10^{15} cm^{-3} for the geometries used, i.e. the influence of thermotranspiration can be neglected. In all of the rf ion storage devices described in section III.B, there is a density gradient of the target gas from the center to the ends of the trap. To minimize this effect and to determine absolute rate coefficients, correction electrodes, indicated in Figure 7, are used to concentrate the ion cloud in the center of the ion trap where the pressure is measured.

As discussed in section II, the effective rate coefficient for an association reaction comprises a radiative and a ternary component, which increases proportionally to the density as can be seen from eq 16. Therefore, to accurately determine these two components it is advisable to vary the density of the stabilizing partner over the range where the product $k_3n = k_r$. For association reactions examined in the presence of buffer gas, the effective rate coefficient depends on the density of the reactant, e.g. H_2, and the third body which can either be the reactant or a buffer gas (usually He). Effective rate coefficients for association reactions with a buffer gas are determined by fixing the reactant gas at a low density (10^{10}–10^{12} cm^{-3}) and recording the increase of additional product ions as a function of the density of the added buffer gas. This procedure is illustrated in more detail in section IV.A for the association reaction of $H^+ + H_2$.

The actual temperature of the neutral gas in the ion trap is determined by the temperature of the trap electrodes and the walls of the surrounding environment (concerning the geometry, see Figure 4). This temperature also determines the actual density of the target gas. A test which is very sensitive to the He density is the ternary association reaction $He^+ + 2He \rightarrow He_2^+ + He$, shown in Figure 11, which has been carefully examined over the temperature range 30–300 K in a liquid helium cooled drift tube.[34] Using these published absolute values as a calibration reference, the actual target density in the ring electrode ion trap can be calculated from the measured relative increase $\Delta N_2/N_1\Delta t$ of helium dimer ions using eq 33. Comparison of this density with the pressure measured at room temperature leads directly to the actual temperature (eq 34). Corresponding experiments have been performed at several nominal temperatures, two examples of which are included in Figure 11 (solid circles). At the lowest nominal temperature of the cold head, 10 K, this procedure has led to an actual reaction temperature

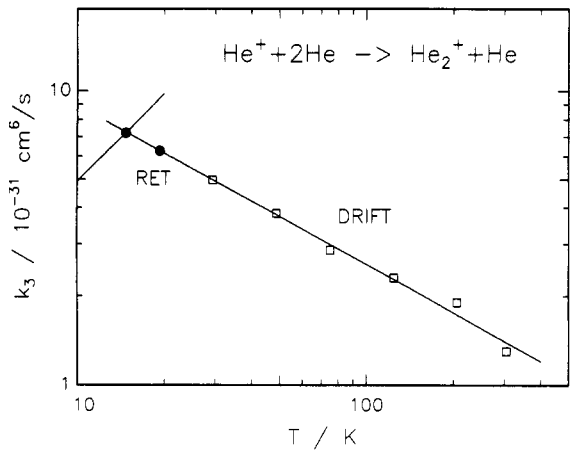

Figure 11. Calibration of the ion temperature in the ring-electrode trap using the $He^+ + 2He$ ternary association reaction. According to the results (open squares) from a low-temperature ion drift tube experiment,[34] the ternary rate coefficients vary proportionally to $T^{-0.54}$. The ion-trap results (solid circles), measured at low temperatures, have been adjusted to this curve by using the actual temperature as an adjustable parameter. The slanted error bar shows the uncertainty caused by the density–temperature dependence.

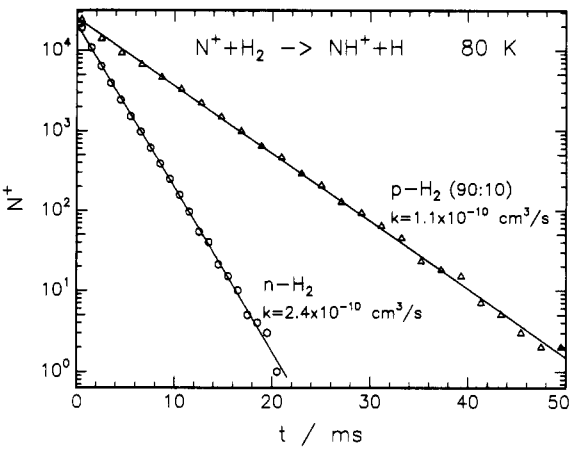

Figure 12. Attenuation of N^+ ions due to the endothermic bimolecular reaction $N^+ + H_2(j = 0,1) \rightarrow NH^+ + H$ for normal hydrogen (circles) and 90% enriched para hydrogen determined in the ring-electrode trap at 80 K. The variation of the signal over 5 decades and the accumulation time of a few minutes indicate the high sensitivity of the apparatus.

of 15 K. If the temperature was actually 10 K, a ternary rate coefficient of 5×10^{-31} cm^6/s would result from the measured ion intensities. The effect of the uncertainty of the temperature (and therefore on the density) is illustrated using the slanted error bar in Figure 11.

In the preceding example, the unknown energy distribution of the ions may also play a role since the collision temperature, T_{coll}, is a function of both the "temperature" of the ions and the temperature of the target gas. For the collision process $A^+ + B$ the collision temperature is determined by the masses

$$T_{coll} = (m_{A^+}T_B + m_B T_{A^+})/(m_{A^+} + m_B) \qquad (35)$$

It is evident from this relation that for the $He^+ + He$ case, T_{coll} is determined equally by the neutral and the ion temperature, while for $m_{A^+} \gg m_B$ the target gas determines predominantly the collision temperature. In a similar manner, based on the published[52,53] temperature-dependent rate coefficient for the endothermic reaction $N^+ + H_2 \rightarrow NH^+ + H$, it was also concluded[42] that the actual H_2 temperature in the ion trap deviates at maximum by 10 K at a nominal temperature of 25 K.

At low temperatures, the rate coefficient for the reaction $N^+ + H_2 \rightarrow NH^+ + H$ is very sensitive to the ortho–para ratio of the H_2 target.[53] In Figure 12, the attenuation of N^+ due to reaction with normal-H_2 and para-enriched H_2 (<10% in $j = 1$, determined using 3 + 1 multiphoton ionization via the C state) at 80 K is shown. The measured rate coefficient for reaction with para-enriched H_2, $k = 1.1 \times 10^{-10}$ cm^3/s, is in good agreement with the 80 K rate coefficient calculated from the theoretical values[53] and assuming a para–ortho ratio of 9:1.

The overall accuracy of the measured rate coefficients depends on several parameters including the collision temperature and the reagent gas density, as discussed in the preceding examples. For ions formed in very low abundance, such as in radiative association processes, the statistical errors can become rather large, especially if there is a rather large background at the mass of the association product. Also systematic errors must be considered, for example from hydrogen deuterium exchanging collisions with trace amounts of deuterated impurities in the H_2 reagent. The H_2 reagent employed in these experiments contains an HD impurity estimated to be on the order of 50 ppm. Other problems are caused by reactions with ^{13}C impurities, especially for hydrocarbon ions with more than one carbon atom. For example, the hydrogen-abstraction reaction $^{13}CC_2^+$ with H_2 leads to a product at mass 38, which is identical to the product resulting from the hydrogen-abstraction reaction between C_3H^+ and H_2.

IV. Results

In this section several reaction systems will be discussed which are important for molecular growth in interstellar space. An overview of these reactions has been given in Figure 1 and in section I. The following section A deals with the $H^+ + H_2$ system. This important prototype system is used to illustrate the concepts of complex formation and statistical models, complex lifetime, and radiative processes. Sections B–F describe reactions which are vital links in the hydrocarbon chain of interstellar chemistry, processes which include the formation of the fundamental CH_2^+ ion and the synthesis of the cyclic c-$C_3H_2^+$ ion, as well as some reactions with CO. Results are discussed not only for radiative and ternary association processes, but also for competing bimolecular reactions. Finally in section G, very recent results from a new experimental method which provides direct information on radiative lifetimes of highly excited collision complexes are presented.

A. The H_3^+ Prototype System

Due to the large abundance of hydrogen, the stable H_3^+ molecular ion as well as the $H^+ \cdot H_2$ collision complex play important roles in the chemistry of interstellar clouds. The strongly bound H_3^+ ion is produced by the fast exothermic reaction of H_2^+ with H_2. It acts as an efficient protonator of neutral molecules and contributes to deuterium fractionation via the exoergic reaction $H_3^+ + HD \rightarrow H_2D^+ + H_2$.

$H^+ + H_2$ collisions are important for several reasons. The exothermic proton scrambling reaction

$$H^+ + H_2(j = 1) \rightarrow H^+ + H_2(j = 0) \quad (36)$$

is most probably the only gas-phase process which can convert ortho into para hydrogen at interstellar temperatures.[30] Another interesting collision process is the radiative association reaction

$$H^+ + H_2 \rightarrow H_3^+ + h\nu \quad (37)$$

Since this collision occurs exclusively on the electronic ground state potential surface, the highly excited H_3^+ intermediate can only emit photons via rovibrational transitions. Although this process is not a significant source of H_3^+ ions in interstellar chemistry, it may be an important source of photons and, depending on its rate coefficient, may contribute significantly to the infrared radiation observed in interstellar space. In laboratory experiments which will be discussed in the following, the radiative association process competes with the ternary association

$$H^+ + 2H_2 \rightarrow H_3^+ + H_2 \quad (38)$$

or

$$H^+ + H_2 + He \rightarrow H_3^+ + He \quad (39)$$

Due to the simplicity of the H_3^+ system it is possible to perform ab initio calculations with high accuracy. Thus, good potential surfaces, multipole moments, rovibrational transition frequencies and lifetimes, etc. are available (see refs 54 and 55 and references therein). In the last decade, the infrared spectra of the H_3^+ molecule and its isotopomers have been studied extensively[56-58] and satisfactory agreement between theory and experiment has been obtained for the low-lying levels using standard normal mode assignments. The situation for states lying in the vicinity of the dissociation limit is less clear. Much effort (see for example refs 59 and 60) has been directed toward a better understanding of the complicated infrared photodissociation spectrum which has been measured[61] for highly exited metastable H_3^+ ions (nanosecond < τ_{dis} < microsecond). Tentative assignments of the coarse-grained spectra have been proposed based on power spectra of chaotic trajectories[62] or in terms of local normal modes of periodic orbits.[63]

For a complete understanding of the radiative association process 37 not only the spectroscopic aspects of the infrared emission have to be considered but also dynamic features of the collision process. It is well known from a series of experimental and theoretical studies (see refs 30, 64, and 65 and references therein) that at low energies collisions of H^+ with H_2 lead to the formation of a strongly coupled intermediate complex. Two classical trajectories shown in Figure 13 for a rather short time interval, illustrate two typical situations, a complex with intermediate orbiting (upper part) and a strongly interacting complex (lower part). The depicted trajectories have been started in the complex with a total energy of $E = 0.1$ eV above the dissociation limit and a total angular momentum of $J = 20$. After a typical lifetime of 10^{-11} s the system dissociates. Using a representative set of trajectories, the mean lifetime of H_3^+ complexes, averaged over an adequate range of total angular momenta, has been determined for different total energies.[65] The results have been fitted using an RRKM-like function:

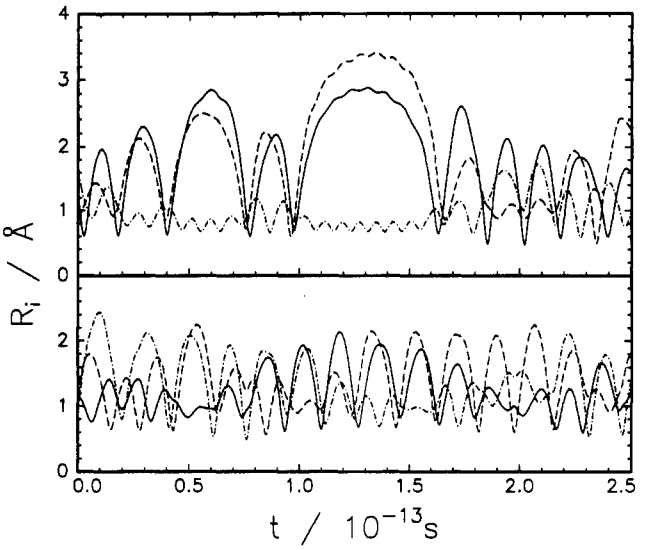

Figure 13. Small time interval of typical classical trajectories for a long-lived $H^+ \cdot H_2$ complex[66] represented as the time dependence of the three distances R_i between the three hydrogen atoms. The trajectories have been started with a total energy $E = 0.1$ eV above the dissociation limit and with a total angular momentum $J = 20$. The upper panel shows a situation with intermediate orbiting, where the third atom remains at large distances during many vibrations of the diatomic. In the lower panel, the frequent crossover between the three distances (minimum exchanges, see ref 64) indicates a strongly interacting collision complex.

$$\tau_{dis} = (1.47 \times 10^{-14})(E + 4.9\ \text{eV}/E)^{1.9}\ \text{s} \quad (40)$$

These rather long-lived collision complexes can be considered as a special class of metastable highly excited H_3^+ molecules and for the understanding of the overall radiative association reaction their emission spectrum and their radiative lifetime must be known. The problem is obviously related to the above-mentioned infrared photodissociation spectrum; however, one should note, that there may be significant differences between those metastable H_3^+ ions (lifetimes between nanoseconds and microseconds) and the $H^+ \cdot H_2$ collision complexes in process 37.

Some very illustrative hints to the frequency range and the rates of spontaneous emission have been derived from a spectral analysis of groups of classical trajectories[67] simulating the $H^+ + H_2$ collision process. In that study the total energy above the dissociation limit was 50 and 100 meV, the time window was about three times longer than that shown in Figure 13. Using an approximate surface for the dipole moment μ, the time dependencies $\mu(t)$ have been calculated. From the spectral analysis of groups of such functions the average dipole spectra have been obtained. These spectra are characterized by a dominant peak at frequencies between 500 and 1000 cm^{-1} (see Figure 2 in ref 67) and a falloff toward a second less pronounced peak at about 3500 cm^{-1}. As can be seen from Figure 13, the low-frequency features may be tentatively attributed to orbiting and large amplitude motions of H^+ relative to H_2 while the higher frequencies are due to vibrations of the perturbed H_2. Note, however, that this characterization of the chaotic trajectories using the picture

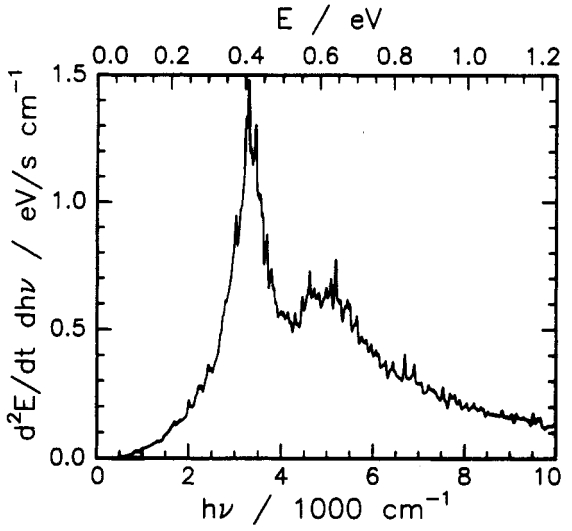

Figure 14. Calculated spectral distribution of spontaneous emission from $H^+ + H_2$ collision complexes.[67] The function derived from classical calculations shows the energy which is emitted by one complex per second and per centimeter^{-1}. The depicted distribution is the average over 80 classical trajectories, calculated at an energy of 0.1 eV above the dissociation limit.

of local bond stretching modes may be misleading and that another analysis, e.g. based on periodic orbits, may be more adequate.

By using classical electrodynamics the spectral distribution of the emitted energy has been calculated from the dipole spectra.[67] A typical result from an average over 80 trajectories is reproduced in Figure 14. Since in the calculation of the spontaneously emitted energy the dipole spectrum is weighted with the fourth power of the frequency, the resulting energy spectrum does not show at all the above described low-energy structures. There is now a rather sharp peak near 3200 cm^{-1} and a very wide peak at about 5000 cm^{-1}. Note that the small amplitude vibrational quanta of H_3^+, ω_1 and ω_2, are 3191 and 2494 cm^{-1}, respectively, and that the vibrational frequency of H_2 is 4162 cm^{-1}. Integration of Einstein's A coefficient over all frequencies has finally yielded[67] an estimate of the radiative lifetime

$$\tau_r(\text{traj}) = 0.14\ \text{ms} \qquad (41)$$

This lifetime is significantly shorter than those calculated[55] for transitions between low-lying states of bound H_3^+. Typical values are 8 ms for the fundamental $\nu_2(E)$ and 6 ms for the first overtone transition.

With the results given in eqs 40 and 41, a theoretical estimate of the radiative association rate coefficient can be calculated from eq 14. In accordance with the above-mentioned, dynamically biased statistical theories[64,68] the complex formation rate coefficient is close to the Langevin rate coefficient

$$k_c = k_L = 2.55 \times 10^{-9}\ \text{cm}^3/\text{s} \qquad (42)$$

Taking $\tau_{dis}(0.1\ \text{eV}) = 2.4 \times 10^{-11}$ s, one obtains

$$k_r(0.1\ \text{eV}) = 4.4 \times 10^{-16}\ \text{cm}^3/\text{s} \qquad (43)$$

Experimental studies of the radiative and three body stabilization of $H^+ \cdot H_2$ and $D^+ \cdot D_2$ were performed in the ring electrode ion trap at 350 and 80 K.[48] The apparatus and the experimental procedure have been

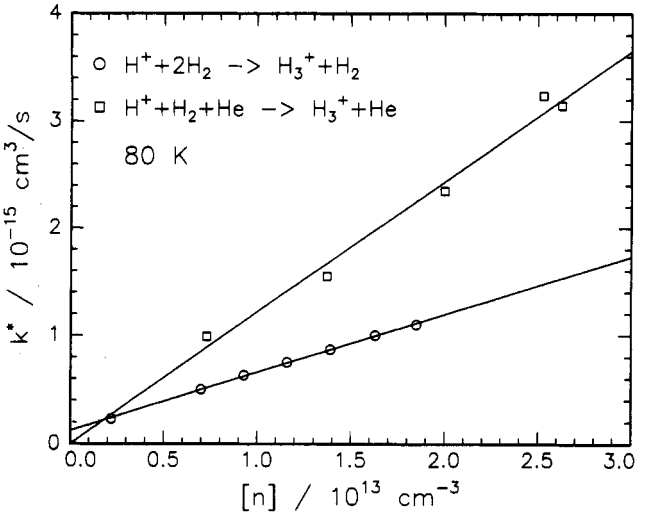

Figure 15. Stabilization of the $H^+ \cdot H_2$ complex with H_2 and He measured at 80 K in the ring-electrode ion trap. The lower line is a fit of $k^* = k_3[H_2] + k_r$ to the data (open circles) measured with pure H_2. The upper line is a fit of $k^* = k_3'$-[He] to data (open squares) measured as a function of added He at a fixed H_2 density. Note that in this case the contribution from $k_3[H_2] + k_r$ has been subtracted. The resulting rate coefficients are given in Table II. The fact that He is a more efficient stabilizer than H_2 is explained in the text.

Table II. Ternary and Radiative Association Rate Coefficients for the Reactions $H^+ + H_2 + M$ (M = H_2 or He) → $H_3^+ + M$ and $H_3^+ + H_2 + M \rightarrow H_5^+ + M$ and the Deuterated Analogs Measured Using the Ring-Electrode Ion Trap (RET)[48]

	RET	
reaction	k_3, cm^6/s 80 K	k_r, cm^3/s 80 K
$H^+ + H_2 + He$	10.7×10^{-29}	
$H^+ + H_2$ (+ H_2)	5.4×10^{-29}	1.3×10^{-16}
$H_3^+ + H_2$ (+ H_2)	2.5×10^{-29}	$<0.5 \times 10^{-16}$
$D^+ + D_2$ (+ D_2)	7.6×10^{-29}	1.0×10^{-16}
$D_3^+ + D_2$ (+ D_2)	3.7×10^{-29}	$<0.5 \times 10^{-16}$

discussed in sections III.B and III.C. A specific problem in this experiment is to completely avoid H_2^+ impurities in the H^+ beam which otherwise would lead to an unwanted H_3^+ background by fast reaction with H_2. As a typical result, Figure 15 shows apparent second-order rate coefficients, k^*, as a function of buffer gas density. The lower curve shows the results (circles) for formation of stable H_3^+ ions using pure H_2 buffer gas. A fit of these data based on eq 16, $k^* = k_3[H_2] + k_r$, yields the three-body rate coefficient and the radiative stabilization rate coefficient given in Table II. The upper curve in Figure 15 shows results (squares) for stabilization of the $H^+ \cdot H_2$ complex with He. In order to study the influence of He, the hydrogen density is held fixed at a rather low value (typically below 10^{13} cm^{-3}) and the H_3^+ signal is measured as a function of the density of additional He. From these data the ternary and radiative contribution for collision with H_2, $k_3[H_2] + k_r$, is subtracted, and one obtains the effective rate coefficient for collisions with He, $k^* = k_3'[He]$. The ternary rate coefficient, k_3', derived from the linear fit is also given in Table II. Included are also results from measurements performed for the deuterated system $D^+ + D_2$.[42]

Table III. H_3^+ Complex and Radiative Lifetimes*

	$f = 0.2^a$	LID[b]	c	d	e
T_{dis}, s	5.5×10^{-11}		5.1×10^{-10}		
T_r, s	1.1×10^{-3}	3.7×10^{-4}		1.4×10^{-4}	$<8 \times 10^{-4}$

* Measurements performed using the ring-electrode ion trap determined from (*a*) ternary and radiative association rate coefficients using a stabilization efficiency $f = 0.2$ and (*b*) laser-induced dissociation (LID).[48] Calculated lifetimes: (*c*) ref 65, (*d*) ref 67, (*e*) ref 14.

It is surprising that the ternary rate coefficient for stabilization with He is larger than that for stabilization with H_2. The difference becomes even more pronounced if one accounts for the differences in the polarizabilities of H_2 and He (see eq 21). Using eqs 11 and 15 and the Langevin rate coefficients

$$k_L(H_3^+ + H_2) = 1.9 \times 10^{-9}\ cm^3/s$$

$$k_L(H_3^+ + He) = 8.2 \times 10^{-10}\ cm^3/s \qquad (44)$$

one obtains from the experimental data of Figure 15 for the ratio of the two stabilization efficiencies

$$f_{He}/f_{H_2} = 4.6 \qquad (45)$$

If for the stabilization with He the upper limit, $f_{He} = 1$, is taken, one obtains for the efficiency of deactivating the intermediate complex $H^+ \cdot H_2$ via a collision with H_2 the upper limit $f_{H_2} = 0.2$. This result seems counterintuitive on the basis of simple statistical arguments discussed in section II, and it is also in contrast to observations for other collision systems where He is less efficient. This unusual behavior can be accounted for if one considers the calculated structures of the H_5^+ molecule.[69] Many of the bound structures can be described by two separate hydrogen molecules with a loosely bound proton in between, and it is therefore conceivable that in certain $H_2 + H^+ \cdot H_2$ collisions the approaching hydrogen has a tendency to pull out the proton from the complex rather than stabilize the complex.

On the basis of the measured ternary rate coefficient and assuming $k_c = k_L$, the lifetime of the collision complex can be estimated from eqs 11 and 15, leading to

$$\tau_{dis} = 1.1 \times 10^{-11}/f_{H_2}\ s \qquad (46)$$

This experimental result, entered in Table III for $f_{H_2} = 0.2$, is 10 times smaller than that predicted from trajectory calculations for a total energy of $E = 20$ meV. There are two explanations for this discrepancy. It must be questioned whether eq 40 can be extrapolated to this low energy where only a very few asymptotic quantum states determine the lifetime in a statistical calculation. From an experimental point of view, it also cannot be excluded that in the present experiment the actual collision energy is somewhat higher. The rf heating effect has been discussed in section III, and it is a special problem for the $H^+ + H_2$ collisions due to the unfavorable mass ratio.

An experimental value for the radiative lifetime is obtained from the measured values for k_3 and k_r. By using eq 17 and $f_{H_2} = 0.2$ yields the result $\tau_r = 1.1$ ms which is (see Table III) 8 times larger than the calculated radiative lifetime ($\tau_r = 0.14$ ms) mentioned above and

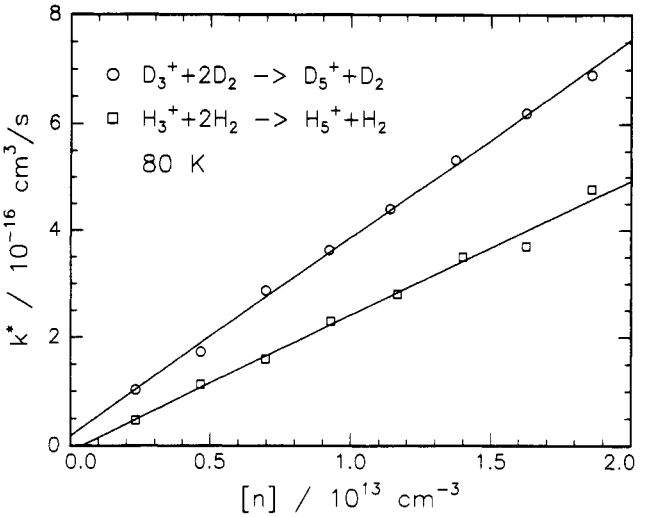

Figure 16. Effective rate coefficients for formation of H_5^+ (open squares) or D_5^+ (open circles) measured at 80 K. The linear fits lead to the results presented in Table II. From an analysis of the errors of both sets of data, only an estimation of the upper limit of the rate coefficients for radiative association can be given.

3 times smaller than the value measured by delayed laser induced dissociation (see section IV.G). These comparisons indicate that, even for this simple prototype system, a more quantitative understanding of the radiative association process requires more experimental and theoretical studies.

An interesting extension of the $H^+ \cdot H_2$ system is to study the influence of the number of degrees of freedom on the radiative association process by adding more hydrogen molecules, i.e. to study the growth of hydrogen clusters. Rate coefficients for the formation of clusters up to H_9^+, which have been determined at 25 K in the ring electrode trap, have been recently reported.[70] As an example Figure 16 shows effective rate coefficients for $H_3^+ \cdot H_2$ and $D_3^+ \cdot D_2$ stabilization as a function of H_2 or D_2 density. The resulting ternary rate coefficients and the upper limits for radiative association are included in Table II. The standard evaluation procedure (eqs 15–17) indicates that the $H_3^+ \cdot H_2$ complex lifetime is shorter

$$\tau_{dis}(H_3^+ \cdot H_2) \sim {}^2/_3 \tau_{dis}(H^+ \cdot H_2) \qquad (47)$$

while its radiative lifetime is slightly larger. The smaller complex lifetime of the five-atom system can be explained with the more than 10 times smaller binding energy of the $H_3^+ \cdot H_2$ intermediate which apparently overcompensates the influence of the additional degrees of freedom.

This result has also some astrophysical relevance since not only $H + H_2$ and $H^+ + H_2$ but also $H_3^+ + H_2$ collisions have been recently considered to play a role in the collision induced generation of interstellar infrared radiation. Comparison of the lifetimes of the $H^+ \cdot H_2$ and the $H_3^+ \cdot H_2$ complexes with the abundances of the two ions reveals that, if at all, only $H^+ + H_2$ collisions have to be considered as a source of infrared radiation.

B. $C^+ + H_2$ Association: Vibrational or Electronic Transitions?

Collisions of C^+ ions with hydrogen atoms or molecules are possible steps in the formation of small

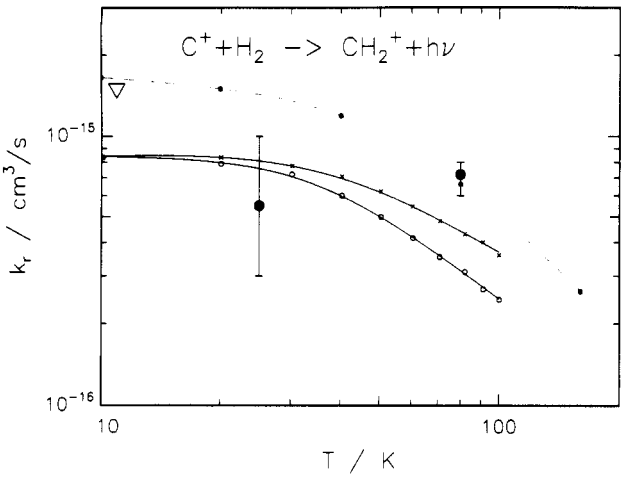

Figure 17. Temperature dependence of the rate coefficient for radiative stabilization of $C^+ + H_2$. The open circles and crosses are predictions from the modified thermal method and from phase-space calculations, respectively.[77] The dashed curve is a similar calculation with tunneling.[78] The triangle is an upper limit value from the Penning trap apparatus.[79] The solid circles represent rate coefficients measured with the 80 K ring-electrode ion trap[48] and the temperature-variable ring-electrode ion trap.[50]

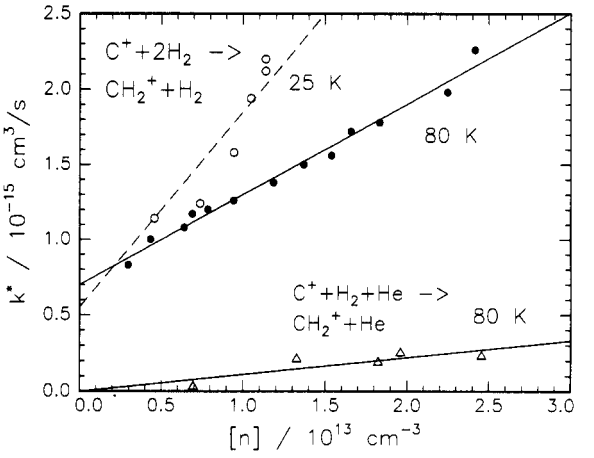

Figure 18. Effective rate coefficients k^* for associative CH_2^+ formation in the temperature-variable ring-electrode ion trap (25 K) and the 80 K ion trap. The two upper curves were recorded using pure hydrogen and provide information on $k_3(H_2)$ and k_r. The data suggest that the radiative association rate coefficients $k_r(25\ K)$ and $k_r(80\ K)$ are smaller than 7×10^{-16} cm^3/s. The bottom curve shows the net influence of additional He acting as the third body. The resulting ternary rate coefficient is compared with other experimental values in Table IV.

hydrocarbons in interstellar chemistry. However, since the reaction $C^+ + H_2 \rightarrow CH^+ + H$ is endothermic by almost 0.4 eV and radiative association of C^+ with H atoms has been estimated to play a negligible role,[71] the only process of importance is the radiative association reaction

$$C^+ + H_2 \rightarrow CH_2^+ + h\nu \qquad (48)$$

To explain observed CH abundances produced by dissociative ion–electron recombination in diffuse clouds, Black and Dalgarno adopted a rate coefficient of $k_r \sim 3 \times 10^{-16}$ cm^3/s for reaction 48.[4]

From a fundamental point of view this triatomic system has many attractive features. As for the H_3^+ system, accurate ab initio quantum chemical calculations are feasible and many features of the potential energy surfaces have been determined.[72,73] Most important for the association reaction is that the complex can be formed without a barrier and it can be effectively stabilized by a rapid electronic transition between the low lying excited $^2B_1$ state and the $^2A_1$ ground state. In a detailed analysis of the radiative association of $C^+ \cdot H_2$, Herbst et al.[74] calculated the transition dipole moment and estimated a radiative lifetime of $\tau_r = 10^{-5}$ s. They also computed the complex lifetime using classical trajectory calculations; however, their value of $\tau_{dis} = 5 \times 10^{-12}$ s was 30 times smaller than that derived from measured three-body rate coefficients[33,75,76] for the reaction

$$C^+ + H_2 + He \rightarrow CH_2^+ + He \qquad (49)$$

In a reinvestigation, Herbst[77] bracketed the radiative association rate coefficient between 10^{-15} cm^3/s $< k_r <$ 10^{-16} cm^3/s. The calculated temperature dependence of the rate coefficient based on results from phase-space theory and from the modified thermal approach is shown in Figure 17. The form of this dependence, especially the leveling off at low temperatures, has been discussed in section II. Also included in this figure are results from similar calculations[78] which account for effects of tunneling. All calculations were performed with the reasonable assumption that mixing of ortho and para hydrogen in the complex does not occur and that the ortho–para ratio is 3:1 at all temperatures. Individual rate coefficients for ortho and para hydrogen are reported to differ by a factor of about three reflecting the differences in the rotational partition functions. The major uncertainty in all these calculations is that there are no reliable estimates of the radiative lifetime, τ_r, indicating the urgent need for experimental work.

The radiative association process has been studied in the Penning ion-trap apparatus described in section III.A. For this very slow reaction, no product ion was detected at 10 K.[79] On the basis of an estimate of the sensitivity of the method used, an upper limit of $k_r <$ 1.5×10^{-15} cm^3/s has been derived. As can be seen from Figure 17 (triangle), this upper limit is in order of magnitude agreement with the calculated rate coefficients.

Further experimental studies have been performed in the 80 K ring-electrode ion trap[48] described in section III.B. The measurements were performed using either pure H_2 or a small amount of H_2 ($<10^{13}$ cm^{-3}) in a He buffer gas at densities between 3×10^{12} and 3×10^{13} cm^{-3}. Apparent second-order rate coefficients obtained are plotted in Figure 18 as a function of target or buffer gas density and a linear fit to the data leads to the ternary rate coefficients given in Table IV. Comparison of these values with results obtained using other methods shows reasonable agreement. The ternary rate coefficient for He is 4.9 times smaller than that for H_2 which is partly due to the differences in the collision rate (see eq 21). Accounting for this difference the stabilization efficiency f_{He} is 1.9 times smaller than f_{H_2}.

The fit in Figure 18 also yields an upper limit value for the radiative association rate coefficient, $k_r(80\ K) = 7 \times 10^{-16}$ cm^3/s. This experimental value is in good accordance with the theoretical predictions shown in Figure 17; however, this may be somewhat fortuitous since the calculated predictions determine separately

Table IV. Ternary Association Rate Coefficients for the Reaction $C^+ + H_2 + M$ ($M = H_2$ or He) $\rightarrow CH_2^+ + M$ Measured Using Flowing Afterglow,[75] Drift Ion Flow Tube,[76] Selected-Ion Flow Tube,[33] Ring-Electrode Ion Trap,[48] and Temperature-Variable Ring-Electrode Ion Trap[50]

reaction	FA:[a] k_3, cm^6/s 90 K	DRIFT:[b] k_3, cm^6/s 80 K	SIFT:[c] k_3, cm^6/s 80 K	RET:[d] k_3, cm^6/s 80 K	RET:[e] k_3, cm^6/s 25 K
$C^+ + H_2 + He$	2.1×10^{-29}		5×10^{-29}	1.2×10^{-29}	
$C^+ + 2H_2$		6×10^{-29}		5.9×10^{-29}	1.3×10^{-28}

[a] Flowing afterglow. [b] Drift ion flow tube. [c] Selected-ion flow tube. [d] Ring-electrode ion trap. [e] Temperature-variable RET.

the quite uncertain quantities k_c, τ_{dis}, and τ_r, the errors of which can compensate each other. The complex and the radiative lifetimes can be determined from the experimental data using eqs 14 and 17. On the basis of a third body stabilization efficiency $f_{H_2} = 0.2$, one obtains a collision complex lifetime of $\tau_{dis} = 1.2 \times 10^{-10}$ s and a radiative lifetime of $\tau_r = 2.6 \times 10^{-4}$ s. Note that this value is 26 times larger than the radiative lifetime used in the theoretical estimates. This rather large lifetime raises the question whether exclusively electronic transitions contribute to radiative stabilization, or whether vibrational transitions are also significantly involved. More remarks on the radiative lifetime of the CH_2^+ complex follow in section IV.G.

Recently, measurements have been extended to lower temperatures using the temperature-variable ring-electrode trap.[50] Some results obtained at a nominal temperature of 25 K and several H_2 densities are included in Figure 18. As discussed in section III.B, measurements performed with this ion trap were affected by several technical problems and the 25 K radiative rate coefficient has a rather large error which is indicated in Figure 17. Therefore, it is not possible to derive a temperature trend from comparison of the two values k_r(25 K) and k_r(80 K). However, a comparison of the ternary rate coefficients, k_3(25 K) $\sim 2k_3$(80 K), clearly indicates that going from 80 to 25 K the complex lifetime becomes larger. This is in accordance with the increase of 2 predicted from the phase space theory (see Figure 17).

The indicated error bars in Figure 17 only account for the scatter of the data. There are other sources of errors which may affect the radiative association rate coefficient. Due to the very small signal rate, it is hard to completely eliminate parasitic reactions, e.g. with gas impurities or traces of metastables, which may lead to background signal on the radiative association product. In the present case, this is especially complicated by the fact that the CH_2^+ radiative association product undergoes fast, exothermic hydrogenation to form CH_3^+. Another process which has to be considered is the endothermic reaction

$$C^+ + H_2 \rightarrow CH^+ + H - 0.398\ eV \qquad (50)$$

The CH^+ ion formed also undergoes rapid reaction with H_2 to give finally CH_3^+. This reaction can be easily observed at elevated temperatures as can be estimated from the phase space prediction $k = \exp(-4575\ K/T) \times 10^{-9}$ cm^3/s.[80] A typical result measured above room temperature is depicted in Figure 19. The rate coefficient, $k = 1.1 \times 10^{-14}$ cm^3/s, indicates an actual trap temperature of 400 K. At temperatures below 100 K this bimolecular reaction is completely negligible; however, it is clear that precautions must be taken in order to avoid ion heating or collisions with nonthermalized H_2 as discussed in section III.

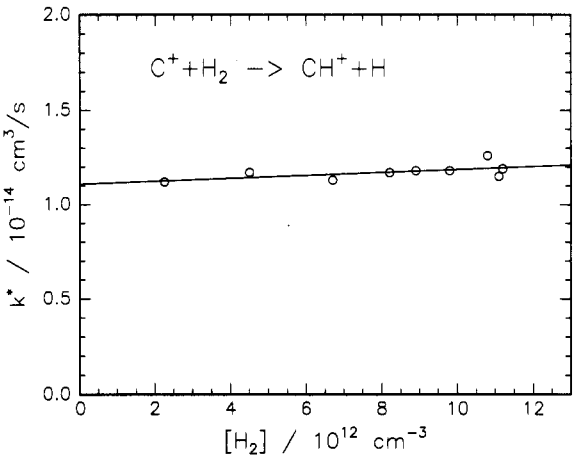

Figure 19. Above room temperature, C^+ reacts predominantly via its endothermic bimolecular channel.[80] The measured rate coefficient, 1.1×10^{-14} cm^3/s, indicates a trap temperature of 400 K. The slight increase of k^* with the H_2 density gives hints to some contributions due to ternary association. Note that, due to fast secondary reactions of CH^+ and CH_2^+ with H_2, CH_3^+ is always the detected ion.

To obtain a reliable low-temperature rate coefficient for the radiative association proces more experimental work is needed. A careful investigation of the temperature dependence would be a crucial test of the theories. The use of pure para hydrogen provides additional insight into the role of nuclear spin statistics. By replacing H_2 with D_2, the influence of the densities of states on the complex lifetime can be probed. This could also influence the radiative lifetimes, provided that vibrational transitions are involved. The question what role the calculated electronically excited potential surfaces of CH_2^+ play in the radiative association process can be possibly answered by spectroscopic studies performed on this molecular ion in the region of the dissociation limit. A first step into this direction will be discussed in section IV.G.

C. Formation of CH_5^+

In the ion chemistry of dense interstellar clouds the CH_3^+ ion and its reaction with H_2 plays a very central role, as can be seen from Figure 2 in the review by D. Smith in this volume.[2] Since hydrogen abstraction to form CH_4^+ is endothermic, the radiative association process

$$CH_3^+ + H_2 \rightarrow CH_5^+ + h\nu \qquad (51)$$

is the only reaction which can occur under interstellar conditions. Because of its importance, this process has attracted the attention of many theorists and experimentalists. However, despite considerable effort on both parts, there are still many conflicting results and interpretations[21,31] which illustrates the situation related to the general understanding of radiative association processes.

Early experimental information on the radiative association process was deduced from measurements of the ternary process

$$CH_3^+ + H_2 + He \rightarrow CH_5^+ + He \qquad (52)$$

at 300 K[82] and later at 80 K.[33] The astrophysical relevance of these experimental data and comparison with "modified thermal" calculations was discussed by Herbst et al.[83] In early models of interstellar molecular synthesis a 10 K value of $k_r = 1.0 \times 10^{-14}$ cm^3/s was used.[84] A direct determination of the radiative rate coefficient, k_r(13 K) = 1.1×10^{-13} cm^3/s, was first achieved in the Penning ion-trap experiment of Barlow, Dunn, and Schauer[20,85] which is described in section III.A. At that time, the agreement between the measured value and theoretical estimates, e.g. k_r(10 K) = 3.3×10^{-14} cm^3/s,[86] was gratifying; however, there was a significant deviation between calculated ternary rate coefficients for $CH_3^+ + H_2 + He$ collisions[83] and the SIFT data.[33,82]

The results from the Penning trap and the SIFT experiments created a lot of theoretical activities. In a series of papers, Bates[87-90] improved details of his theoretical model and used it to reevaluate the measured ternary and radiative rate coefficients. He reasoned that in the SIFT experiment the density was not low enough to avoid saturation and that the use of normal-hydrogen in the Penning experiment led to heating of the ions to a temperature greater than 13 K. The conclusion from these activities[90] was that the radiative lifetime of the $CH_3^+ \cdot H_2$ complex must be shorter than 30 μs and that electronic transitions must play a role in the radiative association. A very recent summary of the different applications of the "modified thermal treatments" to the $CH_3^+ \cdot H_2$ association process has been given by I. W. M. Smith[78] who also extended this model by including effects of quantum mechanical tunneling.

Following the SIFT and Penning trap experiments, new experimental data for the $CH_3^+ + H_2$ association reaction became available.[21,48] These experiments were carried out in the 80 K ring-electrode ion-trap apparatus which is described in section III.B. One of the earliest results obtained[48] is reproduced in the upper panel of Figure 20, and shows the apparent second-order rate coefficient as a function of increasing H_2 density at 80 K. Note that in this experiment the measurements have been extended down to a H_2 target gas density as low as 1×10^{12} cm^{-3} where the product $k_3[H_2]$ becomes comparable with k_r. Additional results have been reported in ref 21, including experiments with para H_2 and with He buffer gas. A summary of the experimental three body and radiative rate coefficients is given in Table V. This table also includes the radiative rate coefficient obtained with the Penning trap[20] and the ternary rate coefficient determined in the SIFT experiment,[33] which agrees with that from the ion-trap experiment within the combined error limits.

The 80 K radiative rate coefficient, $k_r = 6 \times 10^{-15}$ cm^3/s, is 17 times smaller than that obtained from the 13 K Penning ion trap, $k_r = 1.1 \times 10^{-13}$ cm^3/s. A thorough discussion of the possible sources of error in both of these experiments has been given in ref 21. For a temperature change from 80 to 13 K, theories[14,78,90] predict an increase in the rate coefficient by a factor varying between 2.5 and 4.

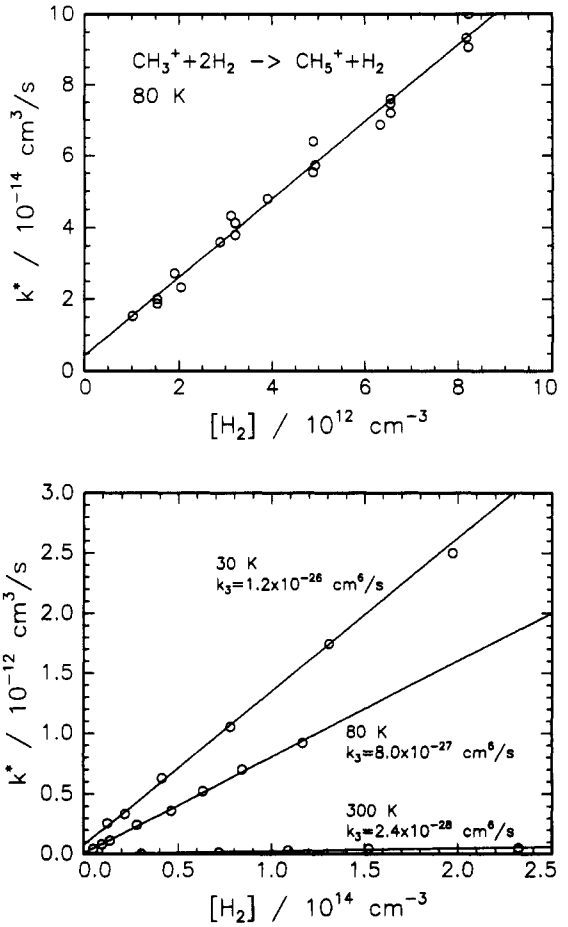

Figure 20. Effective rate coefficients k^* for associative CH_5^+ formation. The upper panel shows early data from the 80 K ring-electrode ion trap.[48] The fit leads to $k_3 = 1.1 \times 10^{-26}$ cm^6/s and $k_r = 4.4 \times 10^{-15}$ cm^3/s which differ slightly from the more recent values[21] given in Table V. The lower panel depicts results recorded with the 22-pole ion trap at three temperatures and at much higher H_2 densities. The derived ternary rate coefficients are listed in Table V. Note that to derive a reliable radiative association rate coefficient, these experiments have to be extended to much lower H_2 densities.

To examine the temperature dependence of the complex lifetime, ternary rate coefficients have recently been measured over a wider temperature range using the temperature-variable 22-pole ion trap described in section III.B. The lower panel of Figure 20 shows apparent second-order rate coefficients as a function of H_2 density at three temperatures, while Figure 21 gives an overview of the temperature dependence of k_3. At elevated temperatures, the T^{-2} dependence of the complex lifetime is consistent with the $T^{-2.3}$ dependence derived from the SIFT data.[33] Note that in the ion trap experiment the complex lifetime is probed with H_2 as third body, while in the SIFT experiment He is used. Both results are consistent with the theoretical prediction that the complex lifetime increases proportional to $T^{-(2.5+\delta)}$ with falling temperature (see section II). As the temperature is decreased below 80 K, this trend levels off, indicating the onset of freezing of the rotational degrees of freedom. This behavior can also be seen from a comparison of the SIFT data (filled squares) with the low-temperature results (stars) measured with the CRESU apparatus.[35] This low-temperature behavior corroborates the theoretical prediction[78] (see dotted line in Figure 21) that the complex

Table V. Radiative and Ternary Association Rate Coefficients for the Reaction $CH_3^+ + H_2 + M$ ($M = H_2$ or He) → $CH_5^+ + M$ Measured Using Penning Ion Trap,[20] Ring-Electrode Ion Trap,[21] Selected-Ion Flow Tube,[33] and 22-Pole Ion Trap

reaction	Penning:[a] k_r, cm³/s 13 K	RET:[b] k_r, cm³/s 80 K	SIFT:[c] k_3, cm⁶/s 80 K	RET:[b] k_3, cm⁶/s 80 K	22-pole:[d] k_3, cm⁶/s 30 K
$CH_3^+ + H_2 + He$			1.5×10^{-27}	0.8×10^{-27}	
$CH_3^+ + H_2$ (+ H_2)	1.1×10^{-13}	6×10^{-15}		8.5×10^{-27}	1.2×10^{-26}
$CH_3^+ + 2H_2$ ($j = 0$)				14.9×10^{-27}	
$CH_3^+ + 2H_2$ ($j = 1$)				6.4×10^{-27}	

[a] Penning ion trap. [b] Ring-electrode ion trap. [c] Selected-ion flow tube. [d] 22-Pole ion trap.

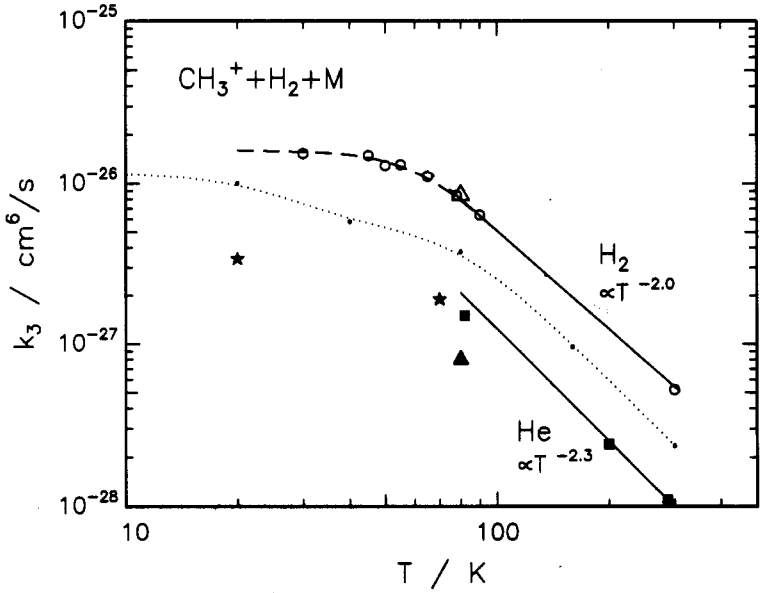

Figure 21. Temperature dependence of the ternary rate coefficient for $CH_3^+ + H_2 + M \rightarrow CH_3^+ + H_2 + M$ ($M = H_2$ or He). The solid squares are SIFT data;[33] the triangles, 80 K ring-electrode ion trap values;[21] and the stars, CRESU data.[35] The large open circles, covering the whole temperature range from 30 to 300 K, are data obtained with the 22-pole ion trap in pure H_2. At temperatures above 80 K the data follow a $T^{-(l/2+b)}$ dependence, while at lower temperatures the measured rate coefficients level off in accordance with predictions (dotted line) from a modified thermal approach.[78]

lifetime at 10 K is at maximum a factor 4 times larger than at 80 K. On the basis of this factor and the upper limit value at 80 K, the radiative association rate coefficient at 10 K is predicted to be smaller than $k_r = 6 \times 10^{-14}$ cm³/s.

Information on the radiative lifetime can be obtained using the standard evaluation method with $k_L(H_2) = 1.57 \times 10^{-9}$ cm³/s and $f_{H_2} = 0.2$. The resulting radiative lifetime, $\tau_r = 4.5$ ms, indicates that the CH_5^+ complex is stabilized by spontaneous emission of infrared photons. In this model (see eq 17) the only uncertainty in the determination of the radiative lifetime is the stabilization rate coefficient, since both k_3 and k_r are measured under identical experimental conditions. This radiative lifetime is in perfect agreement with values measured with other methods (see section IV.G); however, it is in serious conflict with the lifetime given by Bates, $\tau_r = 2.9 \times 10^{-5}$ s.[90] It is evident that more theoretical work is needed to determine radiative lifetimes.

Another unsolved problem is the influence of the initial rotational state of the H_2. There is no doubt that at low temperatures $H_2(j = 0)$ should be more efficient in forming CH_5^+ than $H_2(j = 1)$. Experimental data at 80 K (see Table V) yield a ratio of $k_3(j = 0)/k_3(j = 1) = 2.3$, while the theoretical predictions vary from 9.8[90] to 2.4[78] and are still under discussion.[31] Apparently it does not seem to be straightforward to include restrictions due to the exchange symmetry in statistical models,[29] e.g. to account fully for the conservation of the total nuclear spin of the five H atoms. Other open questions include the role of quantal tunneling and the j-dependent capture cross section caused by the anisotropy of the interaction potential between the ion and the hydrogen molecule.[31]

There is also a need for more experimental work, especially in the temperature range between 10 and 80 K where the determination of the actual internal and translational temperature of the ions is not trivial. Using pure para hydrogen both the influence of nuclear spin conservation and the role of ion heating via rotationally inelastic collisions with $H_2(j = 1)$ could be studied in greater detail. In order to reduce the uncertainty in the radiative rate coefficients, the measurements have to be performed at lower H_2 densities which requires further increase of the sensitivity, reduction of background, and also separate cooling of the ions as explained in Section III.B. As discussed for the $C^+ + H_2$ system, the use of D_2 increases the complex lifetime due to the higher density of states, and also leads to a redshift of the radiation. Low-temperature ion trap studies of partially or fully deuterated $CD_3^+ + D_2$ systems, as performed in a SIFT apparatus,[91] can give additional insight into the role of nuclear spin statistics. Finally, experiments which allow one to extract direct spectroscopic information on the highly excited $CH_3^+ \cdot H_2$ molecular ion, are especially important, and here the reader is also referred to section IV.G.

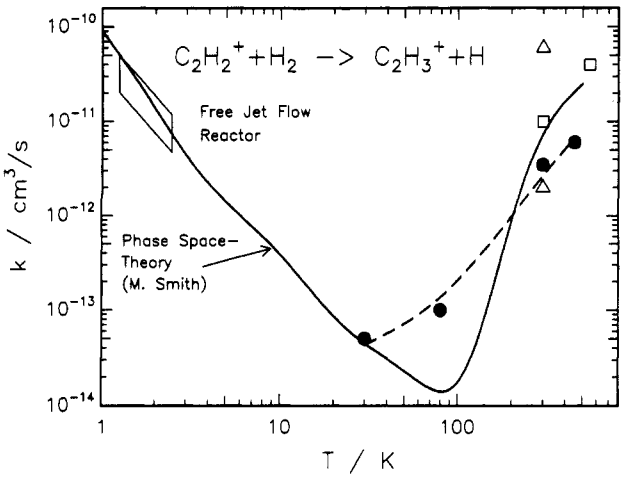

Figure 22. Temperature dependence of the reaction $C_2H_2^+ + H_2 \rightarrow C_2H_3^+ + H$. All experimental results obtained above 80 K indicate endothermic behavior. The two triangles are 300 K ICR values,[92] the lower value is for ground-state ions, the upper one for excited ions. The squares show SIFT results,[93] the solid circles connected with the dashed line are results from ring-electrode and 22-pole ion-trap measurements. The open parallelogram at very low temperatures encloses the majority of the data from Hawley and Smith,[36] who have explained the unexpected temperature dependence using a phase-space model calculation (solid line).

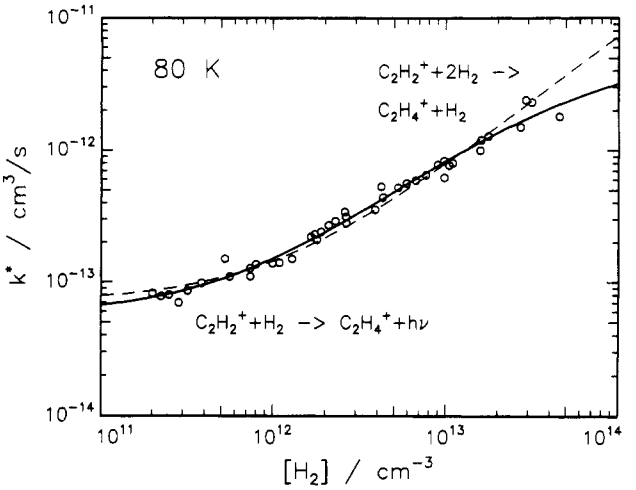

Figure 23. Log/log plot of the effective rate coefficients k^* for associative $C_2H_4^+$ formation as a function of H_2 density. The lines represent fits based on a one-complex model (dashed line) and a two-complex model (solid line). Details are explained in the text.

D. $C_2H_2^+ + H_2 \rightarrow C_2H_4^+$ or $C_2H_3^+ + H$?

In interstellar chemistry the synthesis of hydrocarbons commences with the reactions discussed in sections IV.B and IV.C leading to CH_n molecules. Further reactions of these molecules with C or C^+ lead to more complex hydrocarbons including C_2H which has been detected in interstellar space.[6] A typical fast ion–molecule process is the $C^+ + CH_4$ reaction which produces $C_2H_2^+$ and $C_2H_3^+$ ions. Once formed these ions can undergo further reaction with hydrogen. It has been assumed in interstellar model calculations that the hydrogenation reaction

$$C_2H_2^+ + H_2 \rightarrow C_2H_3^+ + H \qquad (53)$$

is endothermic. This reaction has a long history of study and all measured rate coefficients show in qualitative agreement that $C_2H_3^+$ formation decreases with falling temperature. Several examples from ICR,[92] SIFT,[93] and recent ion-trap measurements are depicted in Figure 22. With the exception of very low temperature data (below 3 K), the relevance of which will be discussed at the end of this section, all these measurements indicate endothermic behavior or at least the existence of a reaction barrier. In addition, appearance potential measurements[94] have also indicated an endothermicity of 2 kcal mol^{-1} for reaction 53. Presuming these conclusions to be correct, the only reaction of interstellar importance between acetylene ions and hydrogen is the radiative association reaction

$$C_2H_2^+ + H_2 \rightarrow C_2H_4^+ + h\nu \qquad (54)$$

In an update of several radiative association rate coefficients, Herbst[14] has proposed for this reaction the temperature dependence

$$k_r = (1.5 \times 10^{-14})(T/300\ \mathrm{K})^{-1}\ \mathrm{cm^3/s} \qquad (55)$$

Later an attempt was made to compare these predictions with estimates based on ternary rate coefficients

$$C_2H_2^+ + H_2 + M \rightarrow C_2H_4^+ + M \qquad (56)$$

measured in a SIFT apparatus (M = He).[95] Examining these attempts, one sees that it is not at all straightforward to extract information on complex formation rate coefficients and complex lifetimes simply from a 80 K ternary rate coefficient. In the following it will be demonstrated that even with a larger set of experimental data, very different conclusions on complex lifetimes can be made, depending on whether one uses a one-complex or a two-complex model as discussed in section II.

$C_2H_4^+$ formation via reactions 54 and 56 has been examined using the 80 K ring-electrode ion trap described in section III.B. The primary ions were generated by electron impact of C_2H_2. The problem of internal excitation of the $C_2H_2^+$ ions and thermalization in the ion trap has been discussed in section III and illustrated in Figure 9. The experiments were performed over a very wide range of H_2 and He densities, so that on the one hand, direct information on radiative association could be obtained, and on the other, the three-body processes could be examined in great detail.

As a first approximation, the data in Figure 23 were evaluated as a fit to the low-density limit $k^* = k_3[H_2] + k_r$ (see eq 16), yielding the two parameters $k_3 = 7.2 \times 10^{-26}$ cm^6/s and $k_r = 7.1 \times 10^{-14}$ s. In a more elaborate evaluation, the measured effective rate coefficients have been used to determine simultaneously all four parameters in the function

$$k^* = k_c\,(k_{H_2}[H_2] + 1/\tau_r)/(1/\tau_{dis} + k_{H_2}[H_2] + 1/\tau_r) \qquad (57)$$

which has been derived from eq 8. The best fit is shown as the dashed line in Figure 23 and has been obtained for the following set of parameters:

$$k_c = 8.6 \times 10^{-10}\ \mathrm{cm^3/s} \qquad \tau_{dis} = 1.5 \times 10^{-7}\ \mathrm{s}$$
$$k_{H_2} = 5.6 \times 10^{-10}\ \mathrm{cm^3/s} \qquad \tau_r = 1.8 \times 10^{-3}\ \mathrm{s}$$

The resulting ternary and radiative rate coefficients are given in Table VI. Evaluation of k_{H_2} using eq 11 leads to a rather large stabilization factor $f_{H_2} = 0.37$. An

Table VI. Radiative and Ternary Association Rate Coefficients for the Reaction $C_2H_2^+ + H_2 + M$ (M = H_2 or He) → $C_2H_4^+ + M$ Measured Using Selected-Ion Flow Tube,[93] Free Jet Reactor,[36] Ring-Electrode Ion Trap, and 22-Pole Ion Trap[e]

reaction	SIFT:[a] k_3, cm^6/s 80 K	free jet:[b] k_3, cm^6/s 2 K	RET:[c] k_3, cm^6/s 80 K	22-pole:[d] k_3, cm^6/s 30 K	RET:[c] k_r, cm^3/s 80 K
$C_2H_2^+ + H_2 + He$	$>7 \times 10^{-27}$		2.0×10^{-26}	1.1×10^{-25}	
$C_2H_2^+ + H_2$ (+ H_2)		4.2×10^{-25}	7.2×10^{-26}	1.8×10^{-25}	7.1×10^{-14}
c1			0.6×10^{-26}		0.4×10^{-14}
c2			8.9×10^{-26}		5.5×10^{-14}
$CH_3^+ + 2p\text{-}H_2$				5.5×10^{-25}	

[a] Selected-ion flow tube. [b] Free jet reactor. [c] Ring-electrode ion trap. [d] 22-Pole ion trap.[e] The radiative and ternary rate coefficients measured at 80 K in the ring-electrode ion trap were determined using the 4-parameter one-complex model and the two-complex model (c1 and c2) described in the text.

equally good fit of the experimental data can be obtained if one fixes the complex formation rate coefficient at the Langevin limit, $k_c = k_L = 1.5 \times 10^{-9}$ cm^3/s, with the slightly different parameters

$$\tau_{dis} = 8.6 \times 10^{-8}\ s \qquad k_{H_2} = 5.6 \times 10^{-10}\ cm^3/s$$

$$\tau_r = 1.8 \times 10^{-3}\ s$$

A comparison of the data points with the best four-parameter fit (dashed line) reveals some minor deviations at intermediate densities. These can be removed if one uses a more complicated model based on the formation of two distinct complexes as discussed in section II. Taking eq 22 and assuming the same radiative lifetimes and stabilization efficiencies for both complexes, six free parameters can be used to fit the data points and one obtains

$$k_{c1} = 1.6 \times 10^{-10}\ cm^3/s \qquad \tau_{dis1} = 4.9 \times 10^{-8}\ s$$

$$k_{c2} = 3.5 \times 10^{-12}\ cm^3/s \qquad \tau_{dis2} = 3.3 \times 10^{-5}\ s$$

$$k_{H_2} = 7.7 \times 10^{-10}\ cm^3/s \qquad \tau_r = 2.1 \times 10^{-3}$$

It can be seen from the solid line in Figure 23, that this function nicely interpolates the data.

This result, the importance of which should not be overestimated, is based on the assumption that two independent complexes are formed with two distinct lifetimes. Since $k_{c1} \gg k_{c2}$, a sequential two-complex model[24] would lead to similar lifetimes. The individual contributions of these two complexes to the ternary and radiative rate coefficients are included in Table VI. Although the longer lived complex is formed with a rate coefficient which is a very small fraction of the Langevin value, it contributes to an extend to more than 90% to the total ternary rate coefficient, $k_3 = 9.5 \times 10^{-26}$ cm^6/s, and the radiative rate coefficient, $k_r = 5.9 \times 10^{-14}$ cm^3/s. The major aim of these examples is to indicate that there is a rather large arbitrariness in extracting information on complex and radiative lifetimes and that very high quality data covering a wide density range are required to gain confidence in the values derived for k_c and τ_{dis}.

For the subject of this review it is important to point out that the derived rate coefficient for radiative association of $C_2H_2^+$ with H_2 is only weakly affected by any of these model assumptions. Indeed, to obtain k_r from the measured effective rate coefficients, contributions from ternary association have to be subtracted. However, these corrections are extremely small since the measurements have been extended to such low H_2 densities that collisional stabilization contributes only to a very minor fraction.

As a final result the rate coefficient for radiative association of $C_2H_2^+$ with normal-H_2 is

$$k_r(80\ K) = 7(^{+2}_{-1}) \times 10^{-14}\ cm^3/s$$

The error limits account for the fact that at the lowest densities the $C_2H_2^+$ ions may not be completely thermalized, although the storage time of 0.5 s has allowed for more than 100 collisions. The agreement with the theoretical value calculated from eq 55, $k_r(80\ K) = 5.6 \times 10^{-14}$ cm^3/s, is probably accidental, but it must be noted that the predicted radiative lifetime of 1 ms[14] is also in accordance with the experimental value for τ_r which varies between 1 and 2 ms, depending on the model chosen.

Very recently it has been questioned whether the radiative association process 54 is of importance at the low temperatures of interstellar clouds, or whether the hydrogen-abstraction reaction 53 may play the more dominant role. The previously mentioned study by Hawley and Smith, performed in a free jet flow reactor,[36] indicated that $C_2H_3^+$ formation may not be endothermic. In order to explain their surprisingly large measured rate coefficients, shown at temperatures of a few Kelvin in Figure 22, these authors have proposed a mechanism which involves a low-temperature switching to a tunneling process. Their calculations, shown as solid line in Figure 22, fits reasonably well all experimental data obtained so far.

A similar phase space calculation incorporating tunneling was recently performed by Yamashita and Herbst.[96] Their calculations were based on an ab initio energy reaction pathway; however, they needed to be corrected to ensure thermoneutrality and to allow for the low-temperature reaction pathway which is required to explain the flow reactor results. Nonetheless, based on this ab initio model, there is a significant discrepancy between this 1–3 K experiment and the rate coefficient measured in the 30 K ion trap. The calculated change in the rate coefficient for reaction 53 between 2 and 30 K is only 1 order of magnitude compared to a factor of 400 between the two experimental results. This discrepancy may be even larger since the ion-trap rate coefficient must be taken as an upper limit. As illustrated in Figure 9, a rather large number of $C_2H_3^+$ ions is formed initially during the thermalization of the $C_2H_2^+$ ions. This background, which also undergoes association to form $C_2H_5^+$, complicates the determination of the rate coefficient for reaction 53. A more

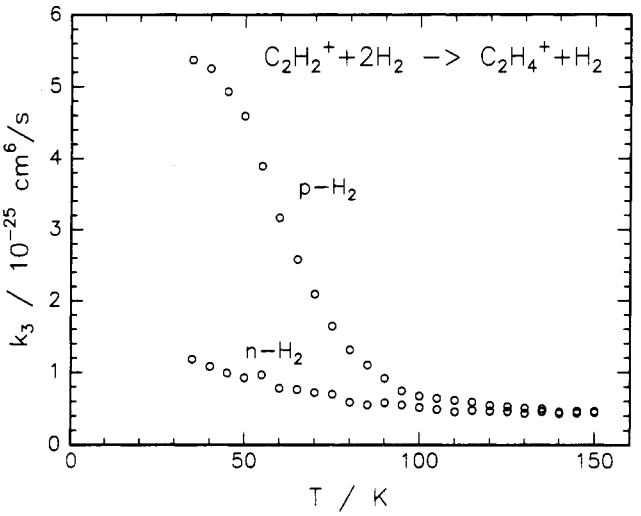

Figure 24. Effect of temperature on the ternary rate coefficient for the reaction $C_2H_2^+ + 2H_2(j = 0,1) \rightarrow C_2H_4^+ + H_2$. The use of para-enriched H_2 (<10% in $j = 1$) leads to a significantly larger rate coefficient in comparison with normal -H_2. Note that the use of $H_2(j = 0)$ as a buffer gas most probably leads to colder ions.

careful investigation of the $C_2H_3^+$ formation in the temperature range accessible to the 22-pole is in progress.

Interesting, as in all reactions with H_2, is the role of ortho and para hydrogen. Theory[96] predicts only a weak dependence on the rotational state. Also the flow experiment[36] could not detect any significant change in either the bimolecular or the termolecular rate coefficient using nuclear spin relaxed hydrogen. In contrast, a recent examination in the 22-pole ion trap lead to the discovery of a significant ortho–para dependence. Figure 24 shows that the three-body association reaction has a weak temperature dependence for normal-H_2, but increases steeply with falling temperature for para-enriched H_2. It is interesting to note that the largest observed value, $k_3(30\ K) = 5.5 \times 10^{-25}$ cm^6/s, is 1 order of magnitude larger than the 3 K value reported in ref 36. Part of these conflicting observations may be due to the fact that $C_2H_2^+ + H_2$ forms complexes with different structures, lifetimes, and barriers, and that the different experiments probe different reaction pathways. Clearly the situation is still clouded and more experiments are needed to determine whether reaction 53 is endothermic or not.

E. $C_3H^+ + H_2$: Hydrogen Abstraction versus Radiative Association

Cyclopropenylidene, c-C_3H_2, the first cyclic molecule to be detected in interstellar clouds,[97] has been proposed to be synthesized by radiative association of C_3H^+ with H_2[24,98]

$$C_3H^+ + H_2 \rightarrow C_3H_3^+ + h\nu \qquad (58)$$

As illustrated in Figure 1, C_3H^+ can be formed via different reactions, e.g. by the reaction of C^+ with C_2H_2.[6] Neutralization of the $C_3H_3^+$ ion by dissociative recombination with electrons may possibly yield both the linear and the cyclic C_3H_2 molecule.

In the last decade reactions of C_3H^+ with H_2 have been actively investigated. In a SIFT study,[24,93] ternary association

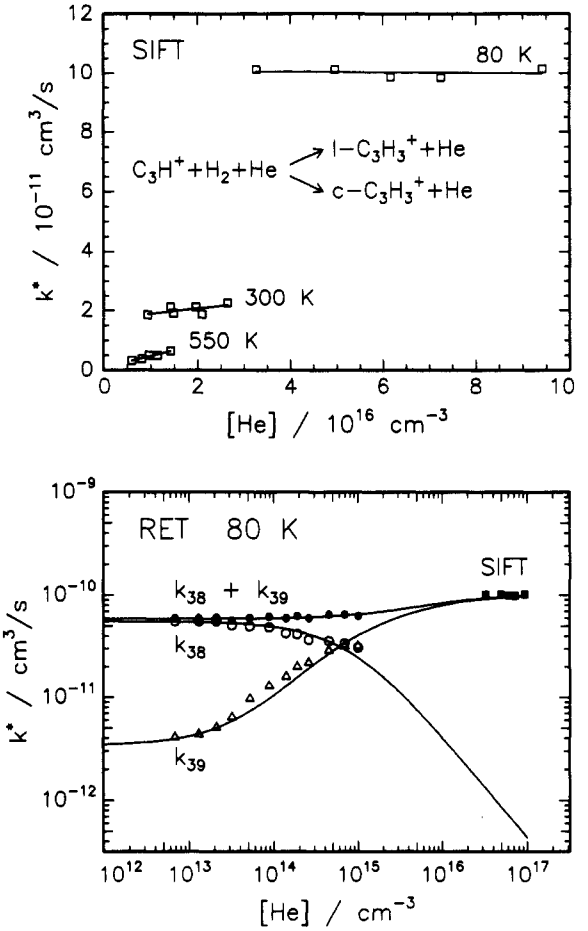

Figure 25. Reaction of C_3H^+ with H_2. The upper panel shows effective rate coefficients k^* for associative $C_3H_3^+$ formation as a function of He density as determined by Smith and Adams in their VT-SIFT apparatus.[24] Only at 550 K is some He density dependence indicated, while at lower temperatures all the complexes formed are stabilized with unit efficiency due to the high He densities in the SIFT experiment (saturation). The lower panel shows ring-electrode ion trap results for the same collision system over an extremely wide He density range at 80 K. Also included are the 80 K SIFT data from the upper panel. At lower densities formation of the association product $C_3H_3^+$ (k_{39}) is suppressed at the expense of the bimolecular product $C_3H_2^+$ (k_{38}). The competition between these two channels is indicated by the fact that the sum $k_{39} + k_{38}$ (solid dots) remains constant over the whole density range. All of the data have been fitted on the basis of an elaborate model described in the text.

$$C_3H^+ + H_2 + He \rightarrow C_3H_3^+ + He \qquad (59)$$

has been identified as the main reaction channel at 300 K and below, while at higher temperatures the hydrogen abstraction reaction

$$C_3H^+ + H_2 \rightarrow C_3H_2^+ + H \qquad (60)$$

becomes dominant. This observation led the authors to the reasonable assumption that reaction 60 is slightly endothermic (~1 kcal/mol) and that in cold interstellar clouds the dominant route to C_3H_2 must be radiative association.

The SIFT experiments are intriguing in that the apparent second-order rate coefficient for reaction 59 is found to be independent of the He gas density at both 80 and 300 K, and only at 550 K is a slight increase evident (see the upper panel of Figure 25). The

astrophysical significance of these results has been discussed in a separate paper,[98] and a tentative value for the radiative association rate coefficient has been estimated to be between 10^{-14} and 10^{-12} cm^3/s. However, the authors also pointed out that it would be necessary to operate at much lower helium densities than are accessible in SIFT experiments in order to distinguish between saturation caused by collisional stabilization and saturation due to radiative association.

In order to directly measure the radiative association rate coefficient, reactions 58–60 have been examined at much lower He densities using the 80 K ring-electrode ion trap.[99] The C_3H^+ ions were generated by electron bombardment of methylacetylene and the ions were typically stored in the ion trap for times up to 100 ms. The hydrogen density was fixed at 5×10^{10} cm^{-3} while the He density was varied between 5×10^{12} and 1×10^{15} cm^{-3}. The rate coefficients for production of $C_3H_3^+$ (k_{39}, reactions 58 and 59) and $C_3H_2^+$ (k_{38}, reaction 60) are depicted in the lower panel of Figure 25 as a function of He buffer gas density. The data have been corrected for minor contributions (at maximum 20%) due to the secondary reaction $C_3H_2^+ + H_2 \rightarrow C_3H_3^+ + H$, which is known to be exothermic[100] but very slow. In a separate experiment, under identical conditions, the rate coefficient for this reaction was determined, $k(80\ \mathrm{K}) = 6 \times 10^{-12}$ cm^3/s.

Remarkably, at low He density the favored reaction for C_3H^+ is hydrogen abstraction to form $C_3H_2^+$ with a rather large rate coefficient. This proves on the one hand the conclusion from Prodnuk et al.[100] that formation of $C_3H_2^+$ is exothermic (6 kcal mol^{-1}). On the the hand, it seems to be in contradiction to the SIFDT[101] results where this channel only could be observed with added kinetic energy. This discrepancy is easy to understand if one compares in Figure 25 the effective rate coefficients for this reaction channel (k_{38}) with the association channel (k_{39}). With increasing He density the effective rate coefficient for $C_3H_2^+$ formation decreases, but this is simultaneously compensated by an increase in the rate coefficient for the formation of the $C_3H_3^+$ product. Interestingly, the sum of the two rate coefficients, $k_{38} + k_{39}$, is almost independent of the He density, yet there is a slight indication of an increase at He densities above 10^{14} cm^{-3}.

For the following interpretation of the results it is assumed that it is significant that the effective rate coefficient, k^*, determined in the SIFT experiment is almost a factor of 2 larger than the sum $k_{38} + k_{39}$. Moreover, it is probably also of importance that in the SIFT experiment two different isomeric forms of the $C_3H_3^+$ product ion have been shown to be produced in equal amounts and these have been designated as the linear and the cyclic structures.[24] If one assumes the existence of these two isomeric forms and if one further accepts that two distinct collision complexes are formed, i.e. c-$C_3H^+ \cdot H_2$ and l-$C_3H^+ \cdot H_2$ (similar to the model described by Smith and Adams[24]), two conclusions for possible reaction mechanisms can be drawn. First, since in general cyclic structures have large binding energies and linear structures are more weakly bound, significant differences in the lifetimes of the two intermediates can be expected. Reactions from the long-lived complex dominate at low densities while the short-lived complex only contributes to k^* significantly at higher densities. Second, it is reasonable to assume that $C_3H_2^+$ reaction products only emerge from the long-lived cyclic complex, because formation of l-$C_3H_2^+$ is known to be endothermic.[100] The differences in lifetime and reactivity can account for all experimental observations provided one assumes in addition that the decay of the cyclic intermediate into products is also very slow.

In order to quantify this speculative interpretation, a rather complicated two-complex model has been invoked.[99] Analogous to the models discussed in section II, separate values of k_c, τ_{dis}, and k_{He} are introduced for each of the intermediates. The radiative lifetime, τ_r, is assumed to be the same for both complexes. Additionally, to account for the formation of the $C_3H_2^+$ product, the reaction rate $1/\tau_{rxn}$ is also introduced. This reaction is only considered for the cyclic intermediate. The model expresses the formation of $C_3H_2^+$ (k_{38}) and $C_3H_3^+$ (k_{39}) using the following equations:

$$k_{38} = k_{c1}(1/\tau_{rxn})/(1/\tau_{dis1} + 1/\tau_{rxn} + k_{He1}[\mathrm{He}] + 1/\tau_r) \quad (61)$$

and

$$k_{39} = k_{c1}(k_{He1}[\mathrm{He}] + 1/\tau_r)/(1/\tau_{dis1} + 1/\tau_{rxn} + k_{He1}[\mathrm{He}] + 1/\tau_r) + k_{c2}(k_{He2}[\mathrm{He}] + 1/\tau_r)/(1/\tau_{dis2} + k_{He2}[\mathrm{He}] + 1/\tau_r) \quad (62)$$

The eight free parameters cannot be largely varied since the values k_{c1} and τ_r can be directly calculated from the low-density asymptotic behavior, and the competition between k_{38} and k_{39} determines τ_{dis1}, τ_{rxn}, and k_{He1}. Inclusion of the SIFT data sets the values of k_{c2}, k_{He2}, and τ_{dis2}; however, it also affects the other parameters. A good fit of all of the data, shown in the lower panel of Figure 25, was obtained for the following set of parameters:

$$k_{c1} = 6 \times 10^{-11}\ \mathrm{cm^3/s} \qquad \tau_{dis1} = 5 \times 10^{-5}\ \mathrm{s}$$
$$k_{He1} = 5 \times 10^{-10}\ \mathrm{cm^3/s}$$

$$k_{c2} = 4 \times 10^{-11}\ \mathrm{cm^3/s} \qquad \tau_{dis2} = 2 \times 10^{-7}\ \mathrm{s}$$
$$k_{He2} = 5 \times 10^{-10}\ \mathrm{cm^3/s}$$

$$\tau_{rxn} = 3 \times 10^{-6}\ \mathrm{s} \qquad \tau_r = 5 \times 10^{-5}\ \mathrm{s}$$

Inspection of these parameters reveals several interesting features of this reaction system which have been discussed in detail in ref 99. The rate coefficients for complex formation, k_{c1} and k_{c2}, are similar but significantly smaller than the Langevin value. This has been explained in ref 24. The unusually long lifetime, $\tau_{dis1} = 50\ \mu$s, is needed to explain the early onset of ternary association observed in the ion-trap experiment. Both complexes are stabilized with high efficiencies. The experimentally observed competition between reaction and stabilization leads to the long reaction time and indicates the existence of a barrier between complex 1 and the $C_3H_2^+$ product. A quantitative analysis of the contributions of the two complexes reveals that the short-lived complex 2 can be almost neglected at the low densities of the trap experiment while both complexes contribute equally to the high density value of the SIFT experiment.

Since at 80 K the $C_3H_2^+$ channel has not been observed in the SIFT experiment,[24] it has been concluded that radiative association is the only route which leads to c-$C_3H_3^+$ formation in interstellar clouds. Indeed, this model and the parameters are in full agreement with the SIFT observation, and explain why at high He densities the $C_3H_2^+$ channel is almost completely (<1%) suppressed. However, under interstellar conditions formation of c-$C_3H_2^+$ occurs with a significant rate coefficient, $k_{38} = 5.5 \times 10^{-11}$ cm^3/s. Since in the presented model these ions originate from complex 1 which is assumed to be cyclic, the resulting c-$C_3H_2^+$ products may contribute significantly to the synthesis of cyclopropenylidene in interstellar clouds.

Despite the fact that, at low densities, $C_3H_2^+$ formation is 20 times faster than $C_3H_3^+$ formation it is interesting to note that the radiative rate coefficient, $k_r = 3.4 \times 10^{-12}$ cm^3/s, is surprisingly large. This is due in part to the extremely long complex lifetime, as well as the short radiative lifetime. This lifetime, $\tau_r = 5 \times 10^{-5}$ s, is shorter than expected for an infrared transition and indicates that an electronic transition may be involved. Note, however, that k_r has to be taken as an upper limit since there are possibly other interfering reactions (see section III.C).

F. Association of CH_3^+ and $C_2H_2^+$ with CO

Reactions of hydrocarbon ions with CO are of keen interest since CO is the second most abundant interstellar molecule (the relative abundance of CO in interstellar clouds is 10^{-4} smaller than the most abundant molecule H_2). It has been proposed[82,102] that radiative association of CH_3^+ (reaction 63) and $C_2H_2^+$ (reaction 64) with CO, followed by electron–ion recombination, is a necessary step in the formation of CH_2CO and C_3O, respectively, which are observed in cold, dense interstellar clouds.[6,103]

$$CH_3^+ + CO \rightarrow CH_3CO^+ + h\nu \quad (63)$$

$$C_2H_2^+ + CO \rightarrow C_2H_2CO^+ + h\nu \quad (64)$$

Atom abstraction with CO is invariably endothermic due to the relatively large C–O bond strength, and proton transfer from most hydrocarbon ions to CO is largely unfavorable due to the low proton affinity of CO. A series of SIFT experiments have shown that ternary association with CO occurs very rapidly for many hydrocarbon ions,[33,104] particularly at low temperature (80 K).[105] However, for many of these reactions, the effective binary rate coefficient is found not to vary with helium pressure, indicating that these reactions most probably proceed in the pressure saturation regime.[104] As discussed in the previous section, experiments performed near saturation complicate the determination of lifetimes or can even lead to erroneous conclusions.

Using the ring-electrode ion trap described in section III.B ternary rate coefficients for the reaction

$$CH_3^+ + CO + He \rightarrow CH_3CO^+ + He \quad (65)$$

have been measured at three temperatures.[106] At 300 and 350 K the effective rate coefficients show a linear dependence, $k^* = k_3$[He], at He densities up to 2×10^{14} cm^{-3}. The derived ternary rate coefficients are listed in Table VII. At 80 K the situation is more complicated since over this range the effective rate coefficient no longer increases proportionally to the He density. This is also indicated in the log/log representation shown in Figure 26. For the determination of k_3 at 80 K only data obtained below 10^{13} cm^{-3} have been evaluated.

Table VII. Ternary Association Rate Coefficients for the Reaction $CH_3^+ + CO + M$ (M = CO or He) → $CH_3CO^+ + M$ Measured Using Ring-Electrode Ion Trap and Selected-Ion Flow Tube[c]

	RET:[a] k_3, cm^6/s	SIFT:[b] k_3, cm^6/s
	$CH_3^+ + CO + He \rightarrow CH_3CO^+ + He$	
350 K	1.4×10^{-27}	1.5×10^{-27}
300 K	2.2×10^{-27}	2.2×10^{-27}
80 K	1.1×10^{-25}	3.9×10^{-26}
	$CH_3^+ + 2CO \rightarrow CH_3CO^+ + CO$	
80 K	2.0×10^{-25}	

[a] Ring-electrode ion trap. [b] Selected-ion flow tube. [c] The 80 K ion flow tube value was deduced from the measured value 1.6×10^{-26} cm^6/s allowing for correction due to saturation effects. See ref 105.

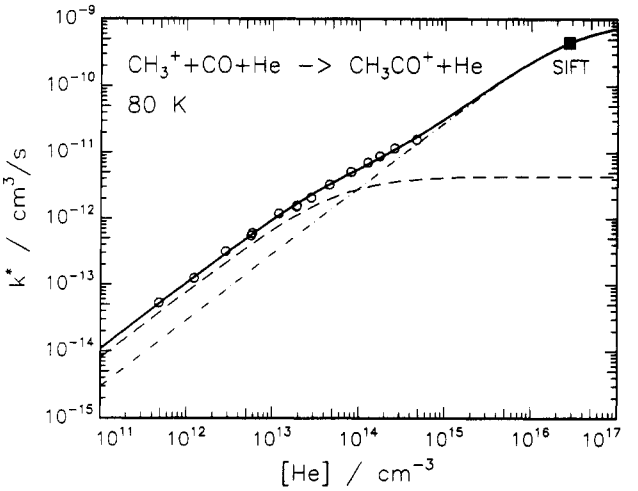

Figure 26. Effective rate coefficients k^* for associative CH_3CO^+ formation as a function of He density. Included are results (open circles) from the 80 K ring-electrode ion trap.[106] The single square is the 80 K SIFT value which has been corrected for saturation effects.[105] The data have been fitted using a two-complex model described in the text. The dashed lines show the individual contributions from the short-lived (dash–dotted) and the long-lived complexes (dashed).

As indicated in Table VII there is very good agreement between the ternary association rate coefficients determined in the ring-electrode ion trap and the SIFT experiment at 300 K and 350 K. Surprisingly, the ternary rate coefficient measured at 80 K in the ion trap deviates only by a factor 2.5 from the deduced SIFT value (i.e. corrected for saturation) although the ion-trap measurements indicate that saturation already occurs at densities which are a factor 1000 below that in the SIFT experiment. A fit of the ion-trap data based on the one-complex model (eq 8) predicts a saturation limit of only 2.7×10^{-11} cm^3/s which is 1 order of magnitude smaller than the measured SIFT value[105] of $k^* = k_3$[He] = [1.6×10^{-26} cm^6/s][2.8×10^{16} cm^{-3}] shown as a solid square in Figure 26. Also in this case the seeming contradiction between the experimental results measured in the two pressure regimes can be solved by invoking a two-complex model. Similar to the C_3H^+ +

H_2 case, one of the two complexes must have such a long lifetime that the onset of saturation already occurs at the low densities of the ion-trap experiment. An unbiased five-parameter fit covering the entire density range was obtained with the function

$$k^* = k_{c1}(k_{He}[He])/(1/\tau_{dis1} + k_{He}[He]) + k_{c2}(k_{He}[He])/(1/\tau_{dis2} + k_{He}[He]) \quad (66)$$

leading to the parameters

$$k_{c1} = 9.5 \times 10^{-10}\ cm^3/s \qquad \tau_{dis1} = 3.1 \times 10^{-7}\ s$$

$$k_{c2} = 4.4 \times 10^{-12}\ cm^3/s \qquad \tau_{dis2} = 1.8 \times 10^{-4}\ s$$

$$k_{He} = 1.0 \times 10^{-10}\ cm^3/s$$

This fit is shown in Figure 26 as a heavy line. Comparison of the stabilization rate coefficient, k_{He}, with the Langevin value, $k_L(He) = 5.6 \times 10^{-10}$ cm^3/s, leads to a reasonable stabilization efficiency, $f_{He} = 0.18$. The rate coefficient for formation of complex 1, k_{c1}, is very close to the Langevin value, $k_L(CO) = 1 \times 10^{-9}$ cm^3/s. Formation of complex 2 is less frequent but due to its long lifetime it plays an important role at low densities. This and the influence of the other parameters on the prediction of measured values can be seen from the following discussion.

The individual contribution of each complex to the effective rate coefficient k^* is plotted in Figure 26. The dashed line indicates that at low densities the main contribution (about 75%) to CH_3CO^+ formation is due to the longer lived complex 2. The very small complex formation rate coefficient, k_{c2}, is more than counterbalanced by the extremely long complex lifetime, τ_{dis2}. As soon as the He density is increased above 10^{14} cm^{-3}, where the collision rate k_{He}[He] approaches the decay rate $1/\tau_{dis2}$, complex 2 reaches its saturation limit. Complex 1 now becomes dominant as can be seen from a comparison of the dashed with the dash-dotted line. At densities above 5×10^{15} cm^{-3}, the contribution to CH_3CO^+ formation from the long-lived complex 2 can be completely neglected, and experiments performed in this density range are insensitive to this channel. At the densities employed in the SIFT experiment saturation also begins to affect the shorter lived channel 1, as indicated by the curvature of the fit. This example demonstrates that SIFT experiments are only sensitive to complexes with lifetimes shorter than 10^{-7} s and that at low densities a small fraction of very long-lived complexes can dictate the reaction behavior.

To more closely examine the radiative association process the $CH_3{\cdot}CO^+$ stabilization has also been studied at 80 K in the absence of helium. As depicted in Figure 27, the effective rate coefficient, k^*, varies linearly with CO density in the range of 5×10^{10} to 5×10^{11} cm^{-3}. A fit to these data yields a ternary rate coefficient, $k_3(80K) = 2.0 \times 10^{-25}$ cm^6/s, and a radiative association rate coefficient of $k_r(80\ K) = 1 \times 10^{-14}$ cm^3/s. A study of possible influences of insufficient thermalization of the CH_3^+ ion indicated[106] that the actual value of k_r may be larger and a value of $k_r(CH_3{\cdot}CO^+) = (3 \pm 2) \times 10^{-14}$ cm^3/s was reported which is significantly smaller than the theoretical prediction of $k_r(80\ K) = 6.7 \times 10^{-13}$ cm^3/s.[14]

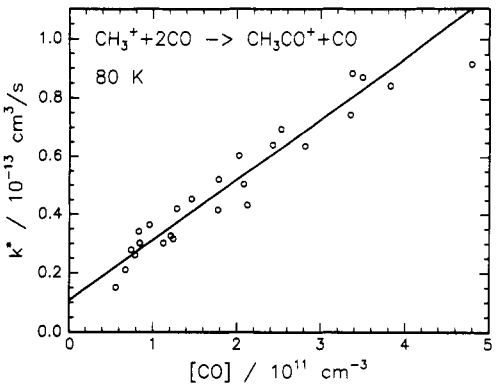

Figure 27. Formation of CH_3CO^+ in a pure low-density CO environment at 80 K. The linear fit leads to a ternary rate coefficient of $k_3 = 2 \times 10^{-25}$ cm^6/s. The measured rate coefficient k^* may be somewhat too small at low CO densities due to insufficient thermalization of the CH_3^+ ions. The consequences for the extracted radiative rate coefficient are discussed in the text.

The measurements have also been extended to higher CO densities[106] and saturation effects were found to occur even earlier than with He buffer gas. An unbiased fit based on the simple one-complex model eq 8 led to the following parameters

$$k_c = 3.9 \times 10^{-12}\ cm^3/s \qquad \tau_{dis} = 2.7 \times 10^{-4}\ s$$

$$k_{CO} = 1.8 \times 10^{-10}\ cm^3/s$$

This result also indicates that the $CH_3{\cdot}CO^+$ products observed at low densities originate predominantly from the long-lived complex which is formed at a very small fraction of the Langevin limit. The stabilization efficiency, $f_{CO} = 0.2$, is consistent with the considerations discussed in section II.

In contrast to the three-parameter fit, the standard evaluation (eq 15, Langevin rates and $f_{CO} = 0.2$) leads to a significantly shorter lifetime, $\tau_{dis} = 1.3$ μs. This two order of magnitude discrepancy is fully explained by the ratio of the complex formation rate coefficients used in the two evaluations. As discussed in context with eq 17, the radiative lifetime is not affected by any model assumptions on k_c or τ_{dis}. Using the measured ternary and radiative association rate coefficients and k_{CO} derived from the one-complex model fit a radiative lifetime of $\tau_r(CH_3{\cdot}CO^+) = 37$ ms is obtained. This radiative lifetime is much longer than the 1-ms value used in ref 14 and is also larger than the 10-ms value estimated with the expression given in ref 8.

The second reaction of interstellar relevance mentioned in the introduction to this section is the association of $C_2H_2^+$ with CO. Some first results obtained at 80 K are depicted in Figure 28. Here the internal energy of the ions, which can be varied by the electron ionization energy and the ion thermalization time, strongly affects the rate of association, as is illustrated by the two sets of data shown in Figure 28. Ions which undergo a larger number of thermalizing collisions exhibit a larger effective rate coefficient than those which experience nearly no thermalizing collisions. The linear fit shown in Figure 28 leads to a ternary rate coefficient of $k_3 = 1.4 \times 10^{-25}$ cm^6/s which is slightly smaller than that determined for CO association with CH_3^+ but almost an order of magnitude larger than the corresponding value measured with He

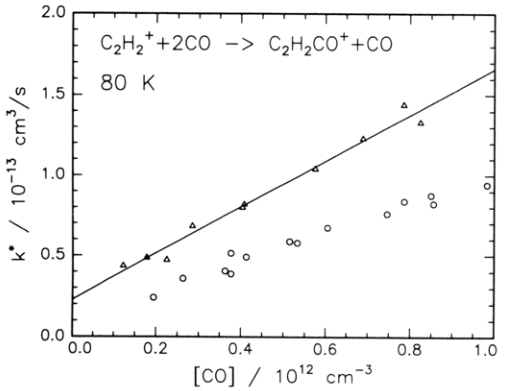

Figure 28. Association of $C_2H_2^+$ in a pure CO environment measured in the ring-electrode ion trap at 80 K. For this system the reactivity strongly depends on the $C_2H_2^+$ internal energy which can be changed by the thermalization time (△, 120 ms; ○, 30 ms). Note that at the lowest density in this experiment the collision rate is about 10^2 s^{-1}. The linear fit leads to a ternary rate coefficient of $k_3 = 1.4 \times 10^{-25}$ cm^6/s and a radiative rate coefficient of $k_r = 2.3 \times 10^{-14}$ cm^3/s.

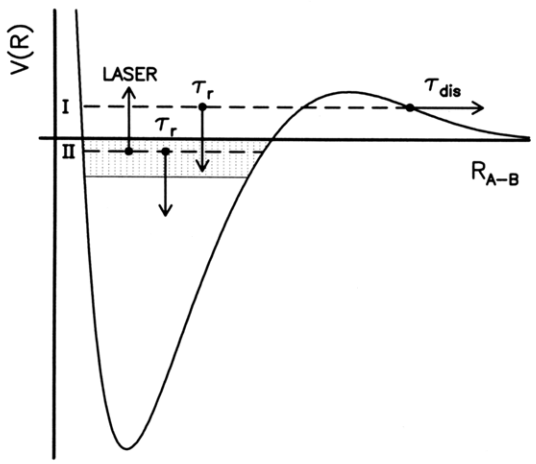

Figure 29. Schematic illustration of two methods (I/II) used for the determination of the radiative lifetime of highly excited molecular ions. The barrier indicates symbolically the lifetime τ_{dis} of the "collision complex". If the molecule is in a metastable state I, dissociation competes with spontaneous emission of an IR photon. The change of population of stable states II can be interrogated by laser-induced fragmentation. By using a CO_2 laser, only a small energy band in the vicinity of the dissociation limit (dotted area) is probed.

buffer.[101] The resulting radiative association rate coefficient, $k_r = 2.3 \times 10^{-14}$ cm^3/s, is in reasonable agreement with a theoretical estimate of $k_\Gamma = 1.5 \times 10^{-14}$ cm^3/s.[14] However, it has to be taken as a lower limit, since the $C_2H_2^+$ ions undoubtedly are not completely thermalized under the conditions of the experiment.

G. Radiative Lifetimes of Collision Complexes

The results for the different reaction systems discussed in the preceding sections have shown that it is not easy to directly determine radiative association rate coefficients needed for application in models of interstellar chemistry, but it is at least in principle technically possible. For a more fundamental understanding of the dynamics of the involved processes, more specific experimental and theoretical information is required. This concerns on the one hand the details of the dynamics of the collision process and, on the other, the spectroscopic aspects of the spontaneous light emission from the intermediate complex.

In the simple model presented in section II the description of the association process was reduced to three parameters, the complex formation rate coefficient, the complex lifetime, and the radiative lifetime. As illustrated in some of the examples, these three parameters cannot always adequately describe the measured apparent second-order rate coefficient k^*, especially over a wide range of density. The introduction of different complex lifetimes could be used to explain some of the experimental observations, and in the case of $C_3H^+ \cdot H_2$, these different complex lifetimes are motivated by different isomeric forms of the intermediate molecule. This observation raises immediately the question whether one single parameter, the radiative lifetime, is really sufficient to provide a representative description of the manifold of all long-lived complex states. It may happen that the emission from different complexes differs by orders of magnitude, e.g. if several potential surfaces are involved, or if high- and low-frequency vibrational transitions occur on the electronic ground state of the complex.

So far in all theoretical treatments of radiative association only a mean value for the radiative lifetime has been used, and most authors have emphasized that the estimated or assumed values contribute significantly to the overall uncertainty of the resulting rate coefficient. Also the experiments performed thus far have led only to a very crude estimate of τ_r, as discussed in sections IV.A–F. It is therefore desirable to perform additional experiments which provide direct spectroscopic insight into the radiative association process.

Several experimental techniques have been developed to measure rates for radiative vibrational relaxation in bound molecules, and several lifetimes in the millisecond range have been reported for low-lying vibrational states.[107,108] It is, however, very questionable whether the properties of these states, where the excitation energy is localized in well-characterized modes, can be used for a description of highly exited states where energy scrambling prevails and where the states are strongly coupled to the dissociation limit. A few related remarks have been made in section II and this problem has also been touched on in section IV.A in the discussion of the spectral properties of the bound H_3^+ molecule and the $H^+ \cdot H_2$ collision complex. From these discussions it was made evident that direct spectroscopic studies of molecules in the vicinity of the dissociation limit are required.

Figure 29 is used to illustrate schematically two methods (I/II) for the determination of radiative and/or dissociative lifetimes of highly excited molecules. Method I starts from a state lying above the dissociation limit. It is assumed that this state is metastable, as symbolized by the barrier in the potential curve. Since the dissociation process, rate $1/\tau_{dis}$, competes with radiative deexcitation, rate $1/\tau_r$, an initial population $N_I(0)$ is partly stabilized and partly transferred into fragments. The total number which undergoes fragmentation in the time interval between $t = 0$ and $t = T$ is given by

$$N_I(T) = N_I(0)\tau_{dis}/(\tau_{dis} + \tau_r)[1 - \exp(-T/\tau)] \quad (67)$$

whereby the total decay rate $1/\tau$ is

$$1/\tau = 1/\tau_{dis} + 1/\tau_r \quad (68)$$

Method II refers to a highly excited but stable state, denoted by II. In this case an initial population $N_{II}(0)$ can only undergo radiative deexcitation and changes according to

$$N_{II}(t) = N_{II}(0) \exp(-t/\tau_r) \quad (69)$$

In order to probe the population $N_{II}(t)$, the method of delayed laser induced dissociation (LID) can be used. Provided that the laser intensity is so low that multiphoton transitions can be ruled out, the energy of a single photon, $h\nu$, determines the energy range of those states which can be dissociated. This range is schematically indicated in Figure 29 by the dotted area. Using a CO_2 laser only those states which are at maximum 0.1 eV below the dissociation limit can undergo photofragmentation.

The two methods described in this simplified manner have been used[42,48] to measure the decay and radiative lifetimes of highly excited molecules and some results for CH_5^+, H_3^+, and CH_2^+ are discussed in the following. The ions of interest have been created in the storage ion source with a pulsed beam of fast electrons. The storage time used in the ion source (a few 100 μs) and the gas mixtures were optimized to limit quenching collisions but to allow for the necessary secondary reaction processes required for the formation of the highly excited ions. Their number was indeed very small but sufficient for the fragmentation studies since the background of fragment ions could be maintained very low. The ion cloud thus prepared was injected into the ring-electrode ion trap and stored for several milliseconds under ultra-high vacuum conditions ($<10^{-9}$ mbar). Under these storage conditions collisional quenching rates are smaller than 1 s^{-1}. Also the ion density ($<10^5$ cm^{-1}) was so low that ion–ion collisions were completely negligible. Any loss of ions by insufficient storage conditions was ruled out on the time scale of interest. Therefore, radiative or dissociative decay processes could be directly observed without interference from any other process.

Highly excited CH_5^+ ions generated from pure methane in the ion source were probed using methods I and II.[48] In experiment I, the results of which are depicted in Figure 30, a fraction of externally created CH_5^+ ions undergoes spontaneous fragmentation. This leads to an increase in the number $N_I(T)$ of CH_3^+ fragments accumulated between the injection and the extraction time T. Although this experiment is performed with a distribution of metastable states, the experimental data can be fitted with the function given in eq 67 using a single lifetime. The non-zero intercept at $T = 0$ is due to some initial CH_3^+ originating from the ion source. Note that the resulting time constant, $\tau(CH_5^+)^* = 5.2$ ms, is a mean value (indicated by the star) and that it is due to both spontaneous dissociation and radiative decay as discussed in the context of eq 68.

In the laser-based dissociation experiment, the injected CH_5^+ ions are probed after a variable storage time by irradiation with an unfocused cw-CO_2 laser for typically 200 μs. The measured fragment intensities, shown in Figure 31, are corrected for minor CH_3^+ contributions (at maximum 10%) from spontaneous decay. Due to the low laser power density (less than

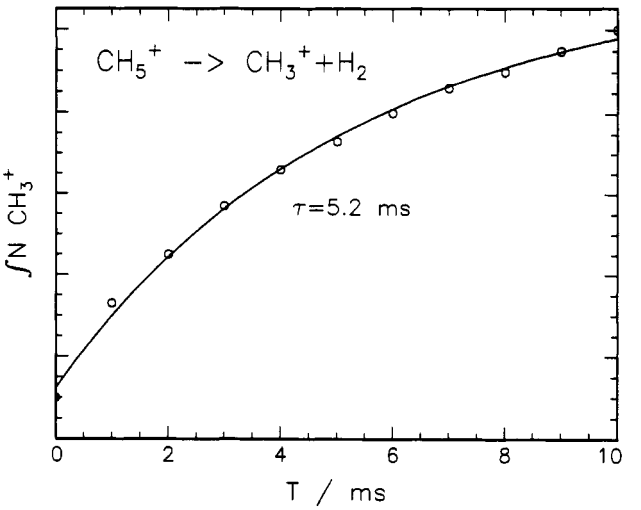

Figure 30. Spontaneous fragmentation of highly excited CH_5^+ ions (corresponds to case I in Figure 29). The plot shows the total number of CH_3^+ fragments integrated in the ion trap during the time $[0,T]$ as a function of T. The fit of the data, using the function given in eq 67, yields $\tau^* = 5.2$ ms. Comparison with the radiative lifetime $\tau_r = 6.2$ ms[42] reveals that the decay rate (eq 68) is predominantly determined by radiative deexcitation and not by depletion via dissociation.

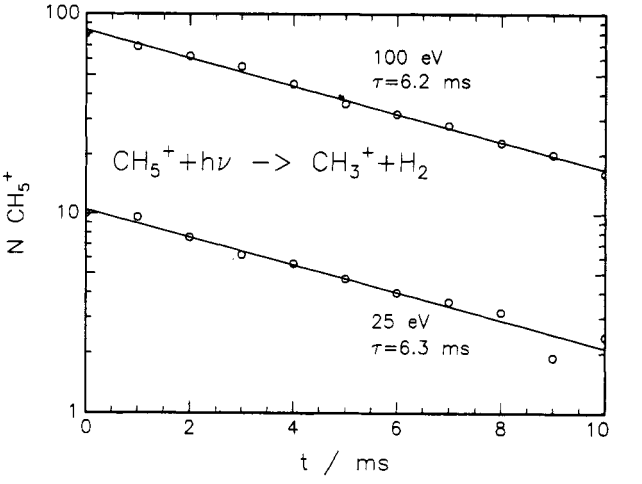

Figure 31. CO_2 laser induced dissociation of highly excited CH_5^+ ions. The plot shows the number of CH_3^+ fragments created with a short laser pulse as a function of the storage time (corresponds to case II in Figure 29). The exponential decline with increasing time yields a radiative lifetime of $\tau_r = 6.2$ ms. An interesting result is that variation of the energy of the ionizing electrons between 25 and 100 eV results only in a change in the total number of ions which can be dissociated, but not in the mean value of the radiative lifetime.

10 W/cm^2) multiphoton processes can most probably be excluded for the small systems reported in this section, although infrared multiphoton decomposition of $C_8H_8^+$ ions has recently been reported to occur even at rather low CO_2 laser power densities.[109] As can be seen from the semilogarithmic representation in Figure 31, the number of laser-induced fragments decreases exponentially with increasing storage time. The two different sets of data indicate that the total number of CH_5^+ ions which can be dissociated increases significantly if the electron energy is raised from 25 to 100 eV; however, in both cases a fit leads to the same time constant.

Since in these experiments the total number of trapped ions remains unchanged and since the only

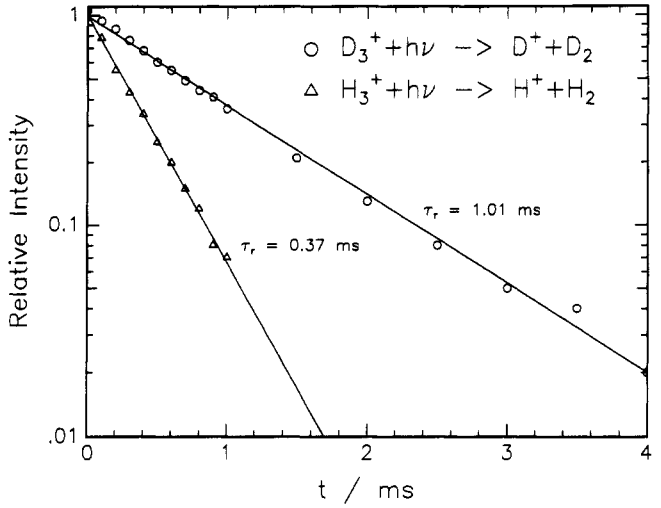

Figure 32. Direct determination of radiative lifetimes of highly excited H_3^{+*} and D_3^{+*} ions using the method of laser induced dissociation. The radiative decay of H_3^+ is 2.73 times faster than for the deuterated ion in accordance with the mass dependence of an infrared transition, $\tau \sim m^{1.5} = 2.83$.

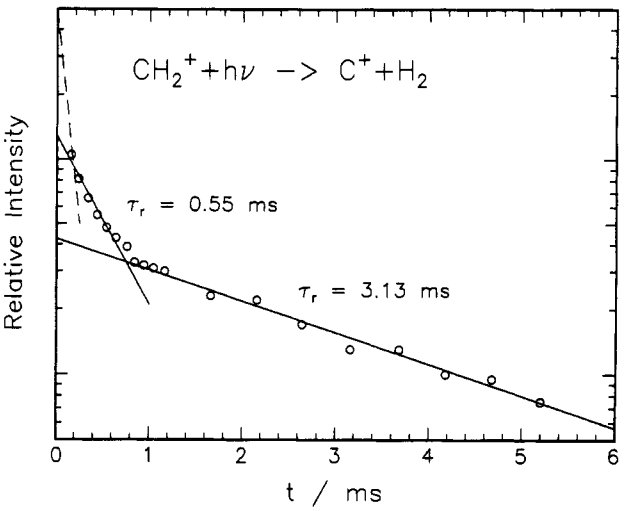

Figure 33. Measurement of the radiative decay of highly excited CH_2^{+*} ions by CO_2 laser induced dissociation. The different lifetimes may be taken as an indication for competition between infrared and electronic transitions. The dashed line below 200 μs indicates symbolically the very short lifetime derived in section IV.B from the measured rate coefficient for radiative association of C^+ with H_2. The microsecond range is outside the time window of the experiment due to the transport of the ions from the ion source to the ion trap.

explanation for the decline of the laser-induced signal is the loss of internal energy by spontaneous emission, this time constant must be due to radiative decay of highly excited CH_5^+ ions, $\tau_r(CH_5^+)^* = 6.2$ ms. Also this measured value is an average over an unknown distribution of excited states, the width of which is determined by the photon energy. In addition, the overall decay process may be slightly affected by the fact that the population of the stable states in region II is influenced by the decaying metastable states I. It is evident that a more precise determination of the radiative lifetimes $\tau_r(E,J,...)$ requires better prepared ensembles of ions, e.g. laser excitation from well-defined lower states.

Within the above-described simple model, the two measured lifetimes can be used to estimate the spontaneous decay lifetime. Equation 68 leads to the large value $\tau_{dis}(CH_5^+)^* = 32$ ms.

The radiative lifetime measured for the highly excited molecules can be compared with the lifetime, $\tau_r(CH_3^+ \cdot H_2) = 4.5$ ms, derived in section IV.C for collision complexes. Although the experiments were performed using different classes of molecules (stable, metastable, and scattering states) the obtained lifetimes are in surprisingly good agreement. This may be taken as an indication that the introduction of a single mean radiative lifetime for strongly coupled states in the vicinity of the dissociation limit is a reasonable approximation. In addition, the lifetimes of the $CH_3^+ \cdot H_2$ collision complexes and the $(CH_5^+)^*$ molecules can be compared with the lifetime of ions in low-lying states. On the basis of ab initio band intensities calculated for CH_5^+,[110] the vibrational radiative lifetime was reported as[31] $\tau_r(CH_5^+(\nu)) = 5.6$ ms. In summary, all these results support the recently published radiative rate coefficient and radiative lifetime of the $CH_3^+ \cdot H_2$ complex.[21]

Similar experiments have also been performed on excited $(H_3^+)^*$ and $(D_3^+)^*$ ions. By using the method of delayed CO_2 laser induced dissociation, a small number of the trapped ions could be fragmented. The time dependence of the relative signal is depicted in Figure 32 for both isotopes. Also in this case, single time constants fully account for the radiative decay of the H_3^+ and D_3^+ ions. The corresponding fits lead to the radiative lifetimes $\tau_r(H_3^+)^* = 0.37$ ms and $\tau_r(D_3^+)^* = 1.01$ ms. The mass dependence of the lifetime is explained on the basis of the fact that the vibrational frequencies of different isotopes are proportional to the square root of the reduced masses, and that the spontaneous photon emission rate is proportional to the third power of the frequency. This simple picture predicts a lifetime ratio, $\tau(\mu_1)/\tau(\mu_2) = 2^{3/2} = 2.8$, which is in good agreement with the measured ratio $\tau(D_3^+)/\tau(H_3^+) = 2.4$. Similar experiments have been performed for CH_5^+ and CD_5^+ [42] and in this case a lifetime ratio of $\tau(CD_5^+)/\tau(CH_5^+) = 2.4$ was determined. This measured ratio is a clear indication of vibrational transitions, since electronic transitions have no mass dependence to a first-order approximation.

The measured radiative lifetime of the exited $(H_3^+)^*$ molecule is smaller than that of the collision complex deduced in section IV.A from the association measurement, $\tau_r(H^+ \cdot H_2)^* = 1.1$ ms, but larger than the lifetime derived from classical trajectory studies.[67] $\tau_r(\text{traj}) = 0.14$ ms. As already discussed, the discrepancies between the two experimental values may be explained by differences in the angular momentum distributions or other characteristics of the two molecular ensembles prepared in the different experiments. The very small theoretical value may be due to an overestimation of the dipole moment surface at small internuclear distances, where the high frequency components of the motion occur.

As a final example of the application of the laser-induced dissociation method, Figure 33 presents results obtained for the $(CH_2^+)^*$ molecule[48] generated by dissociative electron impact ionization of CH_4. In this special case the radiative decay of the states, probed by the CO_2 laser, cannot be fitted with a single lifetime. The two heavy lines, included in the figure, indicate lifetimes in the range 0.5 ms $< \tau_r(CH_2^+)^* <$ 3 ms, while

the dashed line is used to indicate that there may be shorter lifetimes which are outside the time window of the experiment. It is again important to note that these experiments were performed with another manifold of states than those formed in low-energy collisions. If one includes in a comparison the average radiative lifetime derived in section IV.B, $\tau_r(C^+ \cdot H_2)^* = 0.26$ ms, it becomes obvious that in this system both electronic and vibrational transitions may play a role as expected from the ab initio potential surfaces as already discussed in section IV.B.

In the last decade the field of laser-induced processes has grown rapidly, and the examples discussed show that the combination of lasers with ion traps can provide interesting information on the radiative decay of highly excited molecular complexes. There are obviously also other laser applications imaginable which can lead to an improved understanding of the radiative association process, e.g. time-resolved pump and probe experiments. One of the most directly related experiments which is underway in this laboratory, is the laser-induced stabilization of collision complexes. This method will not only provide transition probabilities but also their wavelength dependence.

V. Summary, Conclusions, and Further Developments

In this paper we have presented an overview of the different experimental methods which are used to provide information on rate coefficients for the stabilization of low-energy ion–molecule collision complexes. As illustrated through several examples, most of these experiments operate at high densities where ternary processes dominate and therefore they cannot be used to extract reliable estimates of radiative association rate coefficients. Only ion-trapping techniques can be used to examine ion–molecule reactions at low enough densities that radiative association rate coefficients can be measured directly. Ion cyclotron resonance techniques were first used to examine radiative association reactions; however, only polyatomic ions and neutrals have been studied since they undergo extremely fast radiative association at room temperature. The first low-temperature measurement of a radiative association rate coefficient for a small ion–molecule complex, performed in a Penning trap, demonstrated the utility of ion-trapping techniques for examining ion–molecule reactions of astrophysical interest. In this experimental setup, reactions of an ion cloud could be examined over a period of hours due to the nondestructive detection scheme; however, the method was not sensitive enough to measure rate coefficients for extremely slow processes such as the astrophysically important $C^+ + H_2$ reaction.

The introduction of the temperature-variable rf ion-trap method combined with single ion counting detection has extended the range over which reaction rate coefficients can be examined and values as low as 10^{-17} cm^3/s have been measured using this technique. The wide range of density which can be accessed in the rf ion trap allows radiative as well as ternary association rate coefficients to be measured under identical experimental conditions simply by varying the target gas density. Radiative and ternary association rate coefficients for the reactions examined in this review are summarized in Table VIII. Inspection of the ternary rate coefficients reveals that the rate increases dramatically with increasing molecular complexity. A similar trend is observed for the radiative rate coefficient, where values ranging between 10^{-16} and 10^{-12} cm^3/s are reported. Included in this table are calculated radiative rate coefficients from Herbst.[14] The experimental and theoretical values are in surprisingly good agreement, although this must be considered as fortuitous since the theoretical values were determined using radiative and complex lifetimes which significantly deviate from those derived experimentally. The rather small radiative rate coefficient measured for the association of CH_3^+ with CO does not agree well with the predicted value, but it can be fully accounted for on the basis of the very long radiative lifetime of 37 ms.

The measured density dependence of the apparent second-order rate coefficient and, in some cases, inclusion of data obtained from other methods, was used to derive information on complex lifetimes and radiative lifetimes. The reactions of H^+, C^+, and CH_3^+ with H_2 can be nicely accounted for based on a one-complex model in which an ion–molecule complex with a single mean complex lifetime is formed. As illustrated in Table IX, the complex lifetime increases with the number of degrees of freedom, as expected from statistical considerations. The radiative lifetimes for the $H^+ \cdot H_2$ and $CH_3^+ \cdot H_2$ complexes are typical for vibrational transitions, while the shorter radiative lifetime of the $C^+ \cdot H_2$ complex, $\tau < 1$ ms, can be taken as an indication for radiative stabilization via an electronic transition. Although much longer radiative lifetimes are also observed for the highly excited $(CH_2^+)^*$ molecule, apparently only the fastest decay channel

Table VIII. Summary of Ternary and Radiative Association Rate Coefficients for the Reactions Presented in This Review

reactants	RET:[a] k_3, cm^6/s 80 K	RET:[a] k_r, cm^3/s 80 K	calculated value[b] k_r, cm^3/s 80 K
$H^+ + H_2$	5.4×10^{-29}	1×10^{-16}	
$C^+ + H_2$	5.9×10^{-29}	7×10^{-16}	5.2×10^{-16}
$CH_3^+ + H_2$	8.5×10^{-27}	6×10^{-15}	5.8×10^{-14}
$C_2H_2^+ + H_2$	7.2×10^{-26}	7×10^{-14}	5.6×10^{-14}
$C_3H^+ + H_2$	1.1×10^{-25}	3×10^{-12}	1.2×10^{-12}
$CH_3^+ + CO$	2.0×10^{-25}	3×10^{-14}	6.7×10^{-13}
$C_2H_2^+ + CO$	1.4×10^{-25}	2×10^{-14}	1.5×10^{-14}

[a] Actual values derived from experimental measurements using the ring-electrode trap. See section IV for detailed accounts and discussion of possible errors. [b] For comparison, calculated radiative rate coefficients at 80 K are included.[14]

Table IX. Summary of Complex and Radiative Lifetimes for the Reactions Presented in this Review[a]

reactants		τ_{dis}, s	τ_r, s
$H^+ + H_2$		5.5×10^{-11}	1.1×10^{-3}
$C^+ + H_2$		1.2×10^{-10}	2.6×10^{-4}
$CH_3^+ + H_2$		1.7×10^{-8}	4.5×10^{-3}
$C_2H_2^+ + H_2$		1.5×10^{-7}	1.8×10^{-3}
	c1/c2	$4.9 \times 10^{-8}/3.3 \times 10^{-5}$	2.1×10^{-3}
$C_3H^+ + H_2$	c1/c2	$5 \times 10^{-5}/2 \times 10^{-7}$	5×10^{-5}
$CH_3^+ + CO$	c1/c2	$3.1 \times 10^{-7}/1.8 \times 10^{-4}$	3.7×10^{-2}

[a] The first three reactions were evaluated on the basis of the simple model (eqs 14 and 15) using measured radiative and three-body rate coefficients and $f_{H3}2 = 0.2$. The remaining reactions were evaluated using unbiased fits based on one- and two-complex models as described in section IV.

contributes to the measured radiative association rate coefficient.

Association reactions of $C_2H_2^+$ and C_3H^+ with H_2, and CH_3^+ with CO could not be adequately explained using a model based on the formation of a single complex. To account for the experimental data, a model was introduced which assumes the formation of two distinct classes of complexes with different rates of formation and different mean lifetimes. As indicated in Table IX, the lifetimes of these two classes differ by 2 or 3 orders of magnitude. In all of the reactions examined here, the long-lived complex is formed at a very small fraction of the Langevin rate; however, due to its very long lifetime, it contributes significantly to the reaction products observed at low densities.

All of the results on radiative association reported so far are based on the observation of the stabilized product ion, and the question has often been asked whether this is sufficient proof or whether the emitted photon should be detected. In the measurements performed in an rf ion trap, the formation of a single association product ion per second is easy to detect, while experimental observation of the emitted single infrared photon is extremely difficult, if not impossible if one accounts for the collection and detection efficiency. Even if a photon were detected it would be of no greater significance than the detected ion. The only direct proof for radiative stabilization would be to detect the photon in coincidence with the stabilized complex, a rather hopeless venture. There are other, better-suited optical methods based on laser techniques which lead to an improved understanding of radiative association processes. A very recent experimental advance was the direct measurement of the radiative lifetime of the highly excited molecules using laser-induced dissociation. Other spectroscopical methods can also be used to obtain information on the dynamics of the radiative association process, such as stabilization of the collision complex via stimulated emission.

VI. Acknowledgments

This work is the result of a common effort of several people. Dr. G. Kaefer not only developed the first versions of the cooled ion trap, he also performed several of the experiments mentioned here. Dipl. Phys. W. Paul contributed significantly to the construction and tests of the first 10 K trap while Dipl. Phys. A. Sorgenfrei participated in the recent experiments and developed the 22-pole ion trap. S. Horning thanks the Alexander von Humboldt Stiftung for award of a fellowship which made part of this work possible. The authors thank Prof. Ch. Schlier for many contributions and profitable discussions. Financial support of the Deutsche Forschungsgemeinschaft (SFB 276) is gratefully acknowledged.

VII. References

(1) Herbst, E.; Klemperer, W. *Astrophys. J.* **1973**, *185*, 505.
(2) Smith, D. The Ion Chemistry of Interstellar Clouds. *Chem. Rev.* **1992**, this volume.
(3) Williams, D. A. *Astrophys. Lett.* **1979**, *10*, 17.
(4) Black, J. H.; Dalgarno, A. *Astrophys. Lett.* **1973**, *15*, 79.
(5) Herbst, E.; Delos, J. *Chem. Phys. Lett.* **1976**, *42*, 54.
(6) Winnewisser, G.; Herbst, E. *Topics in Current Chemistry*; Springer-Verlag, Berlin 1987; Vol. 139, pp 121–172. Millar, T. J., Williams, D. A., Eds.; *Rate Coefficients in Astrochemistry*; Kluwer: Dordrecht, 1988.
(7) Dunbar, R. C. *Int. J. Mass Spectrom. Ion Processes* **1990**, *100*, 423.
(8) Herbst, E.; Dunbar, R. C. *Mon. Not. R. Astr. Soc.* **1991**, *253*, 341.
(9) Bass, L.; Chesnavich, W. J.; Bowers, M. T. *J. Am. Chem. Soc.* **1979**, *101*, 5493.
(10) Bates, D. R. *J. Phys.* **1979**, *B12*, 4135.
(11) Herbst, E. *J. Chem. Phys.* **1979**, *70*, 2201.
(12) Woodin, R. L.; Beauchamp, J. L. *Chem. Phys.* **1979**, *41*, 1.
(13) Herbst, E. *Chem. Phys.* **1982**, *65*, 185.
(14) Herbst, E. *Astrophys. J.* **1985**, *291*, 226.
(15) Herbst, E.; Bates, D. R. *Astrophys. J.* **1988**, *329*, 410.
(16) McEwan, M. J.; Denison, A. B.; Huntress, W. T.; Anicich, V. G.; Snodgrass, J.; Bowers, M. T. *J. Phys. Chem.* **1989**, *93*, 4064.
(17) Anicich, V. G.; Sen, A. T.; Huntress, W. T.; McEwan, M. J. *J. Chem. Phys.* **1991**, *94*, 4198.
(18) Dunbar, R. C. *Review on Radiative Association.*
(19) Bohme, D. K. PAH and Fullerene Ions and Ion/Molecule Reactions in Interstellar and Circumstellar Chemistry. *Chem. Rev.* **1992**, this volume.
(20) Barlow, S. E.; Dunn, G. H.; Schauer, M. *Phys. Rev. Lett.* **1984**, *52*, 902.
(21) Gerlich, D.; Kaefer, G. *Astrophys. J.* **1989**, *347*, 849.
(22) Gilbert, R. G.; Smith, S. C. *Theory of Unimolecular and Recombination Reactions*; Blackwell: Oxford, 1990.
(23) Clary, D. C.; Dateo, C. E.; Smith, D. *Chem. Phys. Lett.* **1990**, *167*, 1.
(24) Smith, D.; Adams, N. G. *Int. J. Mass Spectrom. Ion Phys.* **1987**, *76*, 307.
(25) Smith, D.; Adams, N. G.; Alge, E. *Chem. Phys. Lett.* **1984**, *105*, 317.
(26) Light, J. C. *J. Chem. Phys.* **1964**, *40*, 3221.
(27) Pechukas, P.; Light, J. C. *J. Chem. Phys.* **1965**, *42*, 3281.
(28) Miller, W. H. *J. Chem. Phys.* **1970**, *52*, 543.
(29) Quack, M. *Mol. Phys.* **1977**, *34*, 477.
(30) Gerlich, D. *J. Chem. Phys.* **1990**, *92*, 2377.
(31) Bates, D. R. *Astrophys. J.* **1991**, *375*, 833.
(32) Smith, D.; Adams, N. G. *Adv. At. Mol. Phys.* **1988**, *24*, 1.
(33) Adams, N. G.; Smith, D. *Chem. Phys. Lett.* **1981**, *79*, 563.
(34) Böhringer, H.; Arnold, F. *Int. J. Mass Spectrom. Ion Phys.* **1983**, *49*, 61.
(35) Rowe, B. R.; Marquette, J. B.; Rebrion, C. J. *J. Chem. Soc., Faraday Trans. 2* **1989**, *85*, 1631.
(36) Hawley, M.; Smith, M. A. *J. Chem. Phys.* **1992**, *96*, 1121.
(37) Smith, M. A.; Hawley, M. In *Advances in Gas Phase ion Chemistry*; Adams, N. G., Babcock, L. M., Eds.; JAI Press: Greenwich, 1992; Vol. 1.
(38) Herbst, E. *Astrophys. J.* **1991**, *366*, 133.
(39) Barlow, S. E.; Luine, J. A.; Dunn, G. H. *Int. J. Mass Spectrom. Ion Processes* **1986**, *74*, 97.
(40) March, R. E.; Hughes, R. J. *Quadrupole Storage Mass Spectrometry*; Wiley: New York, 1989.
(41) Vedel, F. *Int. J. Mass Spectrom. Ion Processes* **1991**, *106*, 33.
(42) Gerlich, D. *Adv. Chem. Phys.* **1992**, *LXXXII*, 1.
(43) Landau, L. D.; Lifschitz, E. M. *Theoretical Physics*; Pergamon: Oxford, 1960; Vol. 1, p 93.
(44) Dehmelt, H. In *Advances in Atomic and Molecular Physics*; Bates, D. R., Ed.; Academic Press: New York, 1967; Vol. 3, p 53.
(45) Teloy, E.; Gerlich, D. *Chem. Phys.* **1974**, *4*, 417.
(46) Bahr, R.; Teloy, E.; Werner, R. *Verhandl. DGP (VI)* **1969**, *4*, 343.
(47) Gerlich, D. In *Electronic and Atomic Collisions*; Lorents, D. C., et al., Eds.; Elsevier: Amsterdam, 1986; p 541.
(48) Kaefer, G. Dissertation, Freiburg, 1989.
(49) Gerlich, D.; Kaefer, G. *Proceedings of 5th Int. Swarm Seminar*; Adams, N. G., Smith, D., Eds.; Birmingham University: Birmingham, 1987; p 133.
(50) Paul, W. Diplom Thesis, Univ. Freiburg, 1990.
(51) Ikezoe, Y.; Matsuoka, S.; Takebe, M.; Viggiano, A. *Gas Phase Ion-Molecule Reaction Rate constants Through 1986*; Ion Reaction Research Group of The Mass Spectroscopy Society of Japan: Tokyo, 1986.
(52) Marquette, J.; Rebrion, C.; Rowe, B. *J. Chem. Phys.* **1988**, *89*, 2041.
(53) Gerlich, D. *J. Chem. Phys.* **1989**, *90*, 127.
(54) Meyer, W.; Botschwina, P.; Burton, P. *J. Phys. Chem.* **1986**, *84*, 891.
(55) Carney, G. D.; Porter, R. N. *J. Phys. Chem.* **1976**, *65*, 3547.
(56) Carrington, A. *J. Chem. Soc., Faraday Trans. 2* **1986**, *2*, 1089.
(57) Tennyson, J.; Sutcliffe, B. T. *Mol. Phys.* **1984**, *51*, 887.
(58) Oka, T. In *Molecular Ions, Spectroscopy, Structure and Chemistry*; Miller, T. A., Bondybey, V. E., Eds.; North Holland: Amsterdam, 1983.
(59) Pollak, E.; Schlier, Ch. *Acc. Chem. Res.* **1989**, *22*, 223.
(60) Henderson, J. R.; Tennyson, J. *Chem. Phys. Lett.* **1990**, *173*, 133.
(61) Carrington, A.; Kennedy, R. A. *J. Phys. Chem.* **1984**, *81*, 91.
(62) Gomez Llorente, J. M.; Pollak, E. *Chem. Phys. Lett.* **1987**, *138*, 125.
(63) Pollak, E. *Phil. Trans. R. Soc. Lon.* **1990**, *A 332*, 343.
(64) Gerlich, D.; Nowotny, U.; Schlier, Ch.; Teloy, E. *Chem. Phys.* **1980**, *47*, 245.
(65) Schlier, Ch.; Vix, U. *Chem. Phys.* **1985**, *95*, 401.
(66) Berblinger, M., private communication.
(67) Berblinger, M.; Schlier, Ch. *Mol. Phys.* **1988**, *63*, 779.
(68) Gerlich, D. In *Symposium on Atomic and Surface Physics*; Lindinger, W., et al., Eds.; Univ. Innsbruck: Salzburg, 1982; p 304.

(69) Yamaguchi, Y.; Gaw, J.; Remington, R. B.; Schaefer, H. F., III. *J. Chem. Phys.* **1987**, *86*, 5072.
(70) Gerlich, D.; Kaefer, G.; Paul, W. In *Symposium on Atomic and Surface Physics*; Märk, T. D., Howorka, F., Eds.; Obertraun: University of Innsbruck, 1990; p 332.
(71) Graf, M. M.; Moseley, J. T.; Rouff, E. *Astrophys. J.* **1983**, *269*, 796.
(72) Jaquet, R.; Staemmler, V. *Chem. Phys.* **1982**, *68*, 479.
(73) Liskow, D. H.; Bender, C. F.; Schaefer, H. F., III. *J. Chem. Phys.* **1974**, *61*, 2507.
(74) Herbst, E.; Schubert, J.; Certain, P. *Astrophys. J.* **1977**, *213*, 696.
(75) Fehsenfeld, F. C.; Dunkin, D. B.; Ferguson, E. E. *Astrophys. J.* **1974**, *188*, 43.
(76) Johnson, R.; Chen, A.; Biondi, M. *J. Chem. Phys.* **1980**, *73*, 3166.
(77) Herbst, E. *Astrophys. J.* **1982**, *252*, 810.
(78) Smith, I. W. M. *Astrophys. J.* **1989**, *347*, 282.
(79) Luine, J.; Dunn, G. *Astrophys. J.* **1985**, *299*, L67.
(80) Gerlich, D.; Disch, R.; Scherbarth, S. *J. Chem. Phys.* **1987**, *87*, 350.
(81) Gerlich, D. *J. Chem. Phys.* **1989**, *90*, 3574.
(82) Smith, D.; Adams, N. G. *Astrophys. J.* **1978**, *220*, L78.
(83) Herbst, E.; Adams, N. G.; Smith, D. *Astrophys. J.* **1983**, *269*, 329.
(84) Leung, C. M.; Herbst, E.; Huebner, W. F. *Astrophys. J. Suppl.* **1984**, *56*, 321.
(85) Barlow, S. E.; Dunn, G. H.; Schauer, K. *Phys. Rev. Lett.* **1984**, *53*, 1610.
(86) Bates, D. R. *Astrophys. J.* **1983**, *270*, 564.
(87) Bates, D. R. *Astrophys. J.* **1985**, *298*, 382.
(88) Bates, D. R. *Phys. Rev.* **1986**, *A34*, 1878.
(89) Bates, D. R. *J. Chem. Phys.* **1986**, *85*, 2624.
(90) Bates, D. R. *Astrophys. J.* **1987**, *312*, 363.
(91) Smith, D.; Adams, N. G.; Alge, E. *J. Chem. Phys.* **1982**, *77*, 1261.
(92) Buttrill, S. E.; Kim, J. K.; Huntress, W. T.; LeBreton, P.; Williamson, A. *J. Chem. Phys.* **1974**, *61*, 2122.
(93) Smith, D.; Adams, N. G.; Ferguson, E. E. *Int. J. Mass Spectrom. Ion Processes* **1984**, *61*, 15.
(94) Lias, S. G.; Bartmess, J. E.; Liebmann, J. F.; Holmes, J. H.; Levine, R. D.; Mallard, W. G. *J. Phys. Chem. Ref. Data* **1988**, *17*, 1.
(95) Herbst, E.; DeFrees, D.; McLlean, A. *Astrophys. J.* **1987**, *321*, 898.
(96) Yamashita, K.; Herbst, E. *J. Chem. Phys.* **1992**, *96*, 5801.
(97) Matthews, H. E.; Irvine, W. M. *Astrophys. J.* **1985**, *298*, L61.
(98) Adams, N. G.; Smith, D. *Astrophys. J.* **1987**, *317*, L25.
(99) Horning, S.; Sorgenfrei, A.; Gerlich, D. *J. Phys. Chem.* **1992**, manuscript in preparation.
(100) Prodnuk, S. D.; DePuy, C. H.; Bierbaum, V. M. *Int. J. Mass Spectrom. Ion Phys.* **1990**, *100*, 693.
(101) Herbst, E.; Adams, N. G.; Smith, D. *Astrophys. J.* **1984**, *285*, 618.
(102) Huntress Jr., W. T.; Mitchell, G. F. *Astrophys. J.* **1979**, *231*, 456.
(103) Matthews, H. E.; Irvine, W. M.; Friberg, P.; Brown, R. D.; Godfrey, P. D. *Nature* **1984**, *310*, 125.
(104) Giles, K.; Adams, N. G.; Smith, D. *Int. J. Mass Spectrom. Ion Phys.* **1989**, *89*, 303.
(105) Adams, N. G.; Smith, D. *J. Mass Spectrom. Ion Phys.* **1987**, *81*, 273.
(106) Horning, S.; Gerlich, D.; Smith, D. *J. Phys. Chem.* **1992**, manuscript in preparation.
(107) Heninger, M.; Fenistein, S.; Durup-Ferguson, M.; Ferguson, E. E.; Marx, R.; Mauclaire, G. *Chem. Phys. Lett.* **1986**, *131*, 439.
(108) Wyttenbach, T.; Beggs, C. G.; Bowers, M. T. *Chem. Phys. Lett.* **1991**, *179*, 125.
(109) Dunbar, R. C.; Zaniewski, R. C. *J. Chem. Phys.* **1992**, *96*, 5069.
(110) Komorniki, A.; Dixon, D. A. *J. Chem. Phys.* **1987**, *86*, 5625.